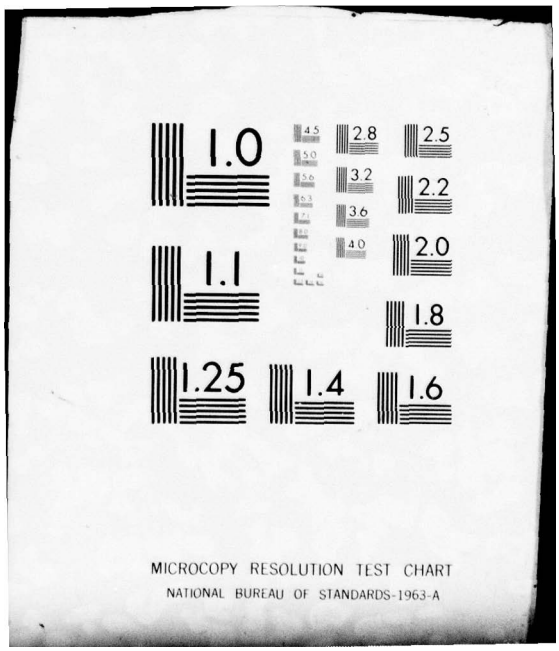
AD-A081 544 DAVID W TAYLOR NAVAL SHIP RESEARCH AND DEVELOPMENT CE--ETC F/G 1/3
EFFECT OF CONFIGURATION ON THE MEASURED PERFORMANCE OF A POWER --ETC(U)
MAR 77 G H KIDWELL, R W GALLINGTON

UNCLASSIFIED DTNSRDC/ASED-380 NL




1.0
1.1
1.25
1.4
1.6
1.8
2.0
2.2
2.5
2.8
3.2
3.6
4.0
4.5
5.0
5.6
6.3
7.1
MICROCOPY RESOLUTION TEST CHART
NATIONAL BUREAU OF STANDARDS-1963-A

LEVEL II gp 2044d

ANVCE (OP-96V)
Rm 800 Commonwealth Bldg.
1300 Wilson Blvd.
Arlington, VA 22209

NW

ADA081544

EFFECT OF CONFIGURATION ON THE MEASURED PERFORMANCE OF A POWER AUGMENTED WING IN GROUND EFFECT

by

George H. Kidwell, Jr. and Roger W. Gallington

APPROVED FOR PUBLIC RELEASE:
DISTRIBUTION UNLIMITED

PRELIMINARY COPY

Report ASED-380

March 1977

DTIC
ELECTE
MAR 1 0 1980
S D
A

DDC FILE COPY

DAVID W. TAYLOR NAVAL SHIP RESEARCH AND DEVELOPMENT CENTER
BETHESDA, MARYLAND 20084

80 2 27 171

UNCLASSIFIED
SECURITY CLASSIFICATION OF THIS PAGE (When Data Entered)

REPORT DOCUMENTATION PAGE

READ INSTRUCTIONS BEFORE COMPLETING FORM

1. REPORT NUMBER: ASED-380
2. GOVT ACCESSION NO.
3. RECIPIENT'S CATALOG NUMBER

4. TITLE (and Subtitle): (6) Effect of Configuration on the Measured Performance of a Power Augmented Wing-in-Ground Effect (U)
5. TYPE OF REPORT & PERIOD COVERED: (9) Preliminary Rept.
6. PERFORMING ORG. REPORT NUMBER

7. AUTHOR(s): (10) George H. Kidwell, Jr.; Roger W. Gallington
8. CONTRACT OR GRANT NUMBER(s): (11) Mar 77

9. PERFORMING ORGANIZATION NAME AND ADDRESS: DTNSRDC, Bethesda, Maryland 20084 (12) 85
10. PROGRAM ELEMENT, PROJECT, TASK AREA & WORK UNIT NUMBERS: PPO (NAVY); TA SSH 15002; WU 1612-009

11. CONTROLLING OFFICE NAME AND ADDRESS: CNO (OP96V), Washington, D.C. 20350
12. REPORT DATE: March 1977
13. NUMBER OF PAGES: 75

14. MONITORING AGENCY NAME & ADDRESS (if different from Controlling Office): (14) DTNSRDC/ASED-380
15. SECURITY CLASS. (of this report)
15a. DECLASSIFICATION/DOWNGRADING SCHEDULE

16. DISTRIBUTION STATEMENT (of this Report): (16) SSH15; (17) SSH15002

Unlimited and approved for Public release.

17. DISTRIBUTION STATEMENT (of the abstract entered in Block 20, if different from Report)

18. SUPPLEMENTARY NOTES

19. KEY WORDS (Continue on reverse side if necessary and identify by block number)

Advanced Naval Vehicle Concepts Evaluation
ANVCE
Technology Assessment
Wing-in-Ground
WIG
Power Augmented
Measured Performance

20. ABSTRACT (Continue on reverse side if necessary and identify by block number)

An analysis is performed to determine the effects of configuration upon the performance of a power augmented ram wing in ground effect (PAR WIG) aircraft. The results of two testing programs are investigated for changes in performance due to changes in flap angle, fan angle, angle of attack, aspect ratio, wing loading, thrust-weight ratio, fan density, and water roughness. Performance is assessed through the vehicle's transport efficiency and heave, along with discussion of the acceleration character-

DD FORM 1 JAN 73 1473 EDITION OF 1 NOV 65 IS OBSOLETE

UNCLASSIFIED
SECURITY CLASSIFICATION OF THIS PAGE (When Data Entered)

387695

20. (cont.)

istics of these varied configurations. Aside from the numerical conclusions which are made concerning the vehicle parametrics, it was found that operation of the vehicle in waves of significant height up to 1/10 span does not significantly degrade a PAR WIG's performance. Numerical results are included to aid performance prediction for a given configuration.

TABLE OF CONTENTS

Page

ABSTRACT . . . . .

ADMINISTRATIVE INFORMATION . . . . .

INTRODUCTION . . . . .

DESCRIPTION OF MODELS . . . . .

TESTING APPARATUS AND PROCEDURE . . . . .

ANALYSIS PROCEDURE . . . . .

GENERAL RESULTS OF THE TESTING PROGRAMS . . . . .

- INTRODUCTION . . . . .
- ASPECT RATIO (A) . . . . .
- ANGLE OF ATTACK (α) . . . . .
- FLAP ANGLE (δ_f) . . . . .
- FAN ANGLE (θ_f) . . . . .
- WING LOADING (W/S) . . . . .
- THRUST-WEIGHT RATIO (T/W) . . . . .
- FAN DENSITY ($^n f/b$) . . . . .
- COMPARISON OF ROUGH AND CALM WATER PERFORMANCE . . . . .
- PARAMETRIC EFFECTS UPON ACCELERATION . . . . .

DISCUSSION AND CONCLUSIONS . . . . .

RECOMMENDATIONS . . . . .

APPENDIX A - DESCRIPTION OF DATA REDUCTION/PLOTTING PROGRAM . . . . .

Accession For
NTIS GRA&I
DDC TAB
Unannounced
Justification
By
Distribution/
Availability Codes
Dist | Avail and/or special
A

80 2 27 171

LIST OF FIGURES

Page

Figure 1 - PAR WIG Model General Arrangement . . . . . .

Figure 2 - Various Wing Planform Sections Available . . . . . .

Figure 3 - Configurations Available for Testing, Planform View .

Figure 4 - Model Flap Configurations . . . . . .

Figure 5 - Model Endplate Configurations . . . . . .

Figures 6a - 6v - Computer-Generated Plots of the Test Results for the Highest - η_T Configurations . . . . .

Figure 7 - Ducted-Fan Flow Model

Figure 8a - Transport Efficiency vs. Aspect Ratio . . . . . .

Figure 8b - Endplate Clearance vs. Aspect Ratio . . . . . .

Figure 9a - Transport Efficiency vs. Fan Angle . . . . . .

Figure 9b - Heave vs. Fan Angle . . . . . .

Figure 10 - Percentage Change in Transport Efficiency Due to Increasing W/S, for Several Aspect Ratios . . . . . .

Figure 11 - Model Acceleration vs. Angle of Attack . . . . . .

Figure 12 - Model Acceleration vs. Flap Angle . . . . . .

Figure 13 - Model Acceleration vs. Fan Angle . . . . . .

Figure 14 - Model Acceleration vs. Wing Loading . . . . . .

Figure 15 - Model Acceleration vs. Thrust-Weight Ratio . . . . .

LIST OF TABLES

Page

Table 1 - Model Configurations and Conditions Tested (of interest) . . . . . .

Table 2 - PAR WIG Model Information . . . . . .

Table 3 - Losses Included in Transport Efficiency . . . . . .

Table 4 - Transport Efficiency & Heave Data with Respect to Aspect Ratio . . . . . .

Table 5 - Transport Efficiency & Heave Data with Respect to Angle of Attack . . . . . .

Table 6 - Configurations Having $\eta_T > 5.0$ . . . . . .

Table 7 - Heave Data with Respect to Flap Deflection Angle . . . . . .

Table 8 - Transport Efficiency & Heave Data with Respect to Fan Angle . . . . . .

Table 9 - Differences in Transport Efficiency due to Wing Loading for Various Aspect Ratios . . . . .

Table 10 - Differences in Transport Efficiency due to Increases in Thrust-Weight Ratio . . . . . .

Table 11 - Transport Efficiency & Heave Data with Respect to Fan Density . . . . . .

Table 12 - Comparison of Extreme-Performance Configurations .

Table 13 - Transport Efficiency & Heave Data for Several Endplate Configurations in 2 Sea States . . . . . .

Table 14 - Recommended & Highest Actual PAR WIG Specifications

NOTATION

Measurements for this investigation were taken in the U.S. Customary System of Units. Equivalent values in the International System (SI) are indicated parenthetically.

A	Wing aspect ratio
A_j	Incoming jet area, ft^2 (m^2)
A_{LE}	Area bounded by the wing leading edge, water surface and endplates, ft^2 (m^2)
b	Wing span, ft (m)
c	Wing chord, ft (m)
h_{EP}	Endplate height, in (cm)
h_w	Wing height, in (cm)[1]
n_f	Number of propulsors (fans)
P	Propulsive power, h_p (W)
$P_{(AIR)}$	Power applied to airstream, h_p(W)
S	Wing area, ft^2 (m^2)
T	Thrust, lb(kg)
T_{EX}	Excess thrust, lb(kg)
V_{CR}	Model cruise (trim) speed, ft/sec (m/sec)
V_j	Jet velocity, ft/sec (m/sec)
V_∞	Freestream velocity, ft/sec (m/sec)
W	Weight, lb (kg)
α	Wing angle of attack, degrees[2]
δ_f	Flap deflection angle, degrees
$\Delta( )$	Increment in some value ( )

η_{AD}	Adiabatic efficiency of propulsor
η_T	Vehicle transport efficiency
ρ	Air density, lb/ft^3 (kg/m^3)
ϵ_f	Fan angle
1	Measured from the undisturbed water surface (or mean water surface in the case of Sea States) to the lower surface of the wing at 38% chord.
2	Measured with respect to the flat bottom surface of the wing and the horizontal.

ABSTRACT

An analysis is performed to determine the effects of configuration upon the performance of a power augmented ram wing in ground effect (PAR WIG) aircraft. The results of two testing programs are investigated for changes in performance due to changes in flap angle, fan angle, angle of attack, aspect ratio, wing loading, thrust-weight ratio, fan density, and water roughness. Performance is assessed through the vehicle's transport efficiency and heave, along with discussion of the acceleration characteristics of these varied configurations. Aside from the numerical conclusions which are made concerning the vehicle parametrics, it was found that operation of the vehicle in waves of significant height up to 1/10 span does not significantly degrade a PAR WIG's performance. Numerical results are included to aid performance prediction for a given configuration.

ADMINISTRATIVE INFORMATION

This parametric investigation was undertaken by the Air ANVCE Projects Division (1612) of the Aviation and Surface Effects Department (16) of the David W. Taylor Naval Ship Research and Development Center (DTNSRDC). The program was sponsored by the Advanced Naval Vehicle Concept Evaluation (ANVCE) Project Office (NOP-96V) of the Program Planning Office (Navy) and was funded under Task Area SSH15002, Work Unit 1612-009.

INTRODUCTION

Recently, significant progress has been made in the area of ground effect flight aided by power augmentation. Sponsored by the Advanced Naval Vehicle Concept Evaluation (ANVCE) since September 1975, studies have been progressing to determine the military worth, technical feasibility, and cost of advanced Wing in Ground effect vehicles (WIGs).

Developments by Gallington (Reference 1) and Gallington and Chaplin (Reference 2) provided a theoretical base for results which had been achieved through earlier tests. This work predicts the limiting performance which is possible when the fundamental geometric aspects of the craft ($A_j/A_{\ell e}$, endplates, ground surface) are properly matched, but certain aspects of the theory are highly idealized. A subsequent testing program by Papadales (Reference 3), which applied the power augmented ram (PAR) phenomenon to a two-dimensional wing with an image, showed that significant increases in lift coefficients, with little reduction in available net thrust, are obtained by power augmentation with respect to conventional operation in ground effect. A similar wind tunnel test, using a two-dimensional flapped wing positioned over a ground board, demonstrated that by properly choosing the height of the wing above the ground, the flap angle, angle of attack of the wing, and propulsor position and angle, performance at least as high as that predicted by the theory was possible at zero forward speed. This test also emphasized the importance of matching the propulsor jet area to the "inlet" area below the wing. While demonstrating that the PAR phenomenon is a highly effective method for performance gain, neither of these tests provided predictions of real-vehicle (primarily non-2D) performance or optimum vehicle configuration.

Two testing programs have since been completed in an attempt to investigate PAR WIG aircraft performance at forward speed over water, and to form a parametric base which provides guidance for vehicle design. The first of these tests, completed in August 1976, provided parametric investigations of a PAR WIG model operating over calm water. This test produced over 1400 data points and provides a great deal of information for aspect ratios of 1/2 to 1 1/2 operating at speeds up to 45 ft/sec (13.7 m/sec). The most recent test (October 1976) performed a parametric investigation of the same model, but operating in various sea states with load alleviation devices (special endplates and flaps). Data was also obtained for many conventional configurations of aspect ratios one and two, operating in calm water and Sea States 4 and 5.

This report is an effort to generate conclusions based upon the parametric data from these tests. The results are analyzed and conclusions formed not only to indicate PAR WIG configurations which show the greatest performance potential, but also to quantify, where possible, performance increments associated with parametric changes, to be used to aid the performance prediction of vehicle candidates. Performance has been judged primarily with the aid of two indicators, the vehicle transport efficiency (a term which combines the lift to drag ratio with the propulsive efficiency) and aircraft flying height or heave. Comment is also made regarding parametric effects upon the model's acceleration characteristics.

MODEL DESCRIPTION

The two testing programs which are dealt with in this report made use of the same basic model, differing primarily in the flap and endplate configurations which were used. This is a parametric model, designed and constructed at DTNSRDC, which allows adjustment of fan angle, number and position of fans, angle of attack, flap angle, endplate size, and aspect ratio. The versatility of this design enabled many different vehicle configurations to be tested in a minimum amount of time. Table 1 provides a listing of the model configurations and conditions which were tested and used for analysis in this report (many from the second test were not used).

A general arrangement two-view drawing of the two-foot (.61 m) span model is shown in Figure 1. The airfoil shape used is an NACA 15 percent four digit airfoil which is cambered such that the bottom surface is flat from the leading edge radius rearward. The model, a 1/30 scale, is designed to have a span of from 2 - 12 feet (.61 - 3.66 m), which yields aspect ratios of from 1/2 to three based on the 4 foot (1.22 m) chord. Seven wing sections were constructed of foam and fiberglass skin, one having a span of 3 feet (.91 m), three having spans of 2 feet (.61 m), and three having 1 foot (.30 m) spans. The planform views of these sections, with cut-outs for the fuselage (fan mounting) bodies, are

shown in Figure 2. All of the sections are made to clamp securely to a 3 1/2-inch (8.87 cm) OD aluminum pipe which passes through the thickest part of the section. By arranging these wing sections on given lengths of pipe, the configurations shown in Figure 3 were formed.

The propulsors for the various model configurations were light-weight 8-inch (20.22 cm) diameter tip-turbine driven fans, powered by compressed air. Depending upon the model aspect ratio and fan density, from 2 to 10 of these fans were mounted in pairs on 49-inch (1.24 m) long 2-inch (5.05 cm) square fiberglass tubing, which served as fuselages. Clamps were manufactured which held each fuselage to the 3 1/2-inch pipe. The two fans were mounted on each fuselage by brackets which allowed fan angles of 0 - 30 degrees and fan positioning at various locations along the fuselage. Combined with the freedom to rotate the fuselage from horizontal to 30 degrees the fan location and angle becomes quite flexible.

Two types of flaps were used on the model. The rigid flap, which was used for the majority of the tests, is simply the aft 0.208c of the airfoil section and is also constructed of fiberglass. The original intent of the design was to have the flap hinge line on the bottom surface of the airfoil 0.167c from the trailing edge and at the center of the circular are separating the flap from the main foil. This would have provided a smooth unbroken surface, even with the flap deflected, to encourage the upper surface flow to remain attached. In construction, however, the flap hinge line ended up where the circular arc intersects the bottom surface. Consequently, any flap deflection caused a serious break in the upper surface contour. undoubtedly resulting in premature separation. Angles of from 0 to 40 degrees were possible with this flap by interchanging aluminum mounting brackets which were fabricated for each angle. The second type of flap (used only in the latter testing program) is a load-alleviation device consisting of a rigid flap, set at a 20^{o} angle, above a flexible airbag having a rigid bottom surface, this surface being deflected a total of 40 degrees when the airbag is inflated. When an impact load is encountered on the flap, the bag is partially deflated by the force, decreasing the angle a maximum of 20^{o}. The wave-energy absorption air was supplied by a fixed-flow electric fan

blowing air into the bag, and the air escape holes could be varied manually. Both flaps are illustrated in Figure 4 although, except for mention in the section dealing with performance comparisons in calm and Sea State conditions, only the rigid flap was used for the purposes of this report.

Five types of endplates were tested in the course of these investigations. The basic rigid endplate is made of fiberglass with a flat-faced forebody planing surface of wood. The bumpers/springs endplate is the basic rigid endplate with the wooden planing surface spring-mounted to act as a wave-impact bumper of either two or four internal springs. The flexible endplate is basically an air-filled plenum with 61 flexible nylon fingers along the lower edge. The metal endplate and shallow-metal endplate are made from 1/4-inch (.63 cm) solid aluminum plate. Figure 5 illustrates these endplate configurations. As with the flaps, only the rigid (metal and shallow-metal) endplates are considered in the majority of this study, the others mentioned in the calm/waves performance analysis section. More details on each of these devices, as well as specifications concerning the other aspects of the model, are provided in Table 2.

TESTING APPARATUS AND PROCEDURE

The two parametric testing programs of the PAR WIG model were conducted at the facilities of the DTNSRDC. The first tests, which were completed by August 1976, were conducted at the Langley Tank 1 (Hampton, Va.), a high-speed towing facility which is operated by the High Performance Craft Powering Branch of the Ship Performance Department. The tank is approximately 2900 feet (883.9 m) long and is filled with brackish water having an approximate density of 63.4 lb per cu foot (1015.5 kg per cu meter). Wave suppressors are located along the sides. The other series of tests, completed in October 1976, were made using the Carderock Carriage 3 (Carderock, Md.), a high-speed towing facility operated by the Experimental Aero-Hydro Group of the Aviation and Surface

Effects Department. The useable dimensions of the tow basin are (at least) 2,110 feet (643.1 m) long, 20 feet (6.1 m) wide, and from 10 to 16 feet (3.0 - 4.9 m) deep. The wavemaker, located at the east end of the tow basin, is of the pneumatic type in which waves are produced by cyclical variation of air pressure on the water surface, and is capable of producing irregular wave spectra which approximate (for the purposes of this test) 1/30 scale Pierson - Moskowitz spectra for fully arisen Sea States 4 and 5.

The model was designed to attach to the carriage by a steel block which was clamped to the pipe at mid-span of each configuration. The model was mounted to a two-inch (5.1 cm) block gage (for drag measurement), which was bolted to a 1 x 2 - inch (2.5 x 5.1 cm) aluminum heave staff. This installation allowed the model to be free in heave, but not in pitch. Drag, heave, and fan RPM's were the variables which were recorded. The earlier testing program also used another method of taking data. This mode involved mounting the model to a six-component dynamometer by way of an aerodynamically-faired strut. The dynamometer incorporates four-inch (10.1 cm) block gages for force and moment measurement. The model was constrained in all directions, however drag, lift, and pitching moment could be measured at various heaves during this segment of the test.

Before testing, a fan calibration was performed. Fan thrust was calibrated against fan RPM and carriage velocity in the following manner. Two fans were mounted horizontally to the dynamometer via the faired strut used in the main test. A series of drive pressures were then tested over the range of carriage speeds desired (0 to 50 ft per sec; 0 to 15.2 m per sec). Measuring fan RPM's, through use of magnetic pick-ups which are mounted in the back of each fan, and the forces transmitted to the dynamometer completed the calibration.

The first testing series was structured into segments roughly corresponding to the different aspect ratio configurations, specifically 1/2, 3/4, 1, and 1 1/2. Further, each of these sections was broken down into free-to-heave runs and dynamometer runs. Table 1 shows a breakdown of the parameters investigated in each of the sections. Note that in

general, speeds of 0, 6, 9, 15, 25, 35 and 45 ft per sec (0, 1.8, 2.7, 4.6, 7.6, 10.7, and 13.7 m per sec) were investigated. Thrust to weight ratios were varied from .15 to .35 and wing loadings from 2.75 to 7.65 lb per sq foot (13.43 to 37.35 kg per sq meter). The angles of attack tested were 0, 2 and 4 degrees.

The latter tests were conducted not only to extend the PAR WIG parametric data base, but primarily to document the performance of three load alleviation devices during the acceleration run of PAR WIG vehicles in irregular head seas. A performance evaluation of these devices is beyond the scope of this parametric analysis (but will be presented in a future report), thus only the data taken for the conventionally-configured model will be discussed. Most of the parameters investigated in this test are the same as those of the earlier program, with the exceptions that only aspect ratios 1 and 2 are used, and that the highest speed tested is 35 ft per sec (10.7 m per sec).

ANALYSIS PROCEDURE

In the power augmented ram wing concept, it seems impossible to clearly separate the power required for lift from the power required for propulsion. This is partly a bookkeeping problem and partly inherent in the concept. For example, the angularity of the flow leaking out under the endplates can either be viewed as a reduction in thrust, as in a conical nozzle rocket, or as an increase in induced drag, as in a non-augmented ram wing. Further, for many of the data points there was considerable excess thrust (expecially at the lower speeds) and a single clean way to define an equivalent L/D for these cases is not possible. During this investigation five apparently correct ways to define equivalent L/D for cases with excess thrust were identified - all yielding different answers. Another complicating feature is that the height of the wing must also be viewed as a desirable performance parameter, and this height is more variable than in the case of an SES, where it is limited by endplate depth, or the case of

an ACV, where it is related to the cushion depth. Because of these complications resulting from the intertwining of lift and propulsion power, the transport efficiency was adopted for analyzing and displaying the powering data.

The analysis procedure is begun by plotting excess thrust, heave, and installed thrust with engines level - all versus speed. The installed thrust with engines level is determined from curve fits of propulsor fan thrust versus velocity at various static RPM's and corresponding regulator pressures. This propulsor calibration data was taken separately with only the propulsion fans, nacelles (aligned with the wind) and their supporting canard-like strut mounted on the block gage. The excess thrust of the completely assembled model (engines inclined) was extrapolated or interpolated (as appropriate) to zero excess thrust (trim speed) by fitting a parabola through the highest three velocities. The heave was extrapolated (or interpolated) to the trim speed by a similar parabolic procedure. The installed thrust at trim speed was obtained from the propulsor calibration curve fit described above. Figures 6a - 6p are plots of some of the configurations demonstrating the greatest potential (Figure 6g is provided for comparison). Knowing trim speed and model weight, the numerator of the transport efficiency is easily calculated through multiplication.

To approximate the power required at trim speed, we assume an appropriate flow model for the fan at an angle to the incoming flow. Figure 7 presents a schematic of this model. We assumed that the fan, at constant supply pressure, generated the same exhaust velocity (more precisely, kinetic energy flux in the exhaust) in the inclined position as it did in the level (aligned) position. This is equivalent to assuming that the gross thrust (defined as momentum flux in the exhaust) is independent of fan inclination. This is a conservative assumption because all of the losses in fan performance associated with the deflection are properly reflected by not reducing the denominator of the transport efficiency. This is a correct accounting procedure because the inclined fans are an essential feature of the PAR concept.

To calculate the power required using the ducted fan flow model,

the values of trim speed and fan static RPM are used to find the installed thrust from the propulsor calibration curves. From the equation for the thrust of a ducted fan,

$$T = \rho V_j A (V_j - V_\infty)$$

$$V_j = \frac{V_\infty + \sqrt{V_\infty^2 + \frac{2T}{\rho A}}}{2} ,$$

the jet velocity is computed. The power added to the airstream in passing through the propulsor is

$$P_{(AIR)} = \rho A V_j \left(\frac{V_j^2}{2} + \frac{V_\infty^2}{2} \right)$$

$$= \eta_{AD} P$$

To address primarily the efficiency of the PAR concept and not that of ducted fans, the ratio

$$\eta_T = \text{transport efficiency} = \frac{WV}{\eta_{AD} P}$$

is used as the primary measure of efficiency. η_{AD} is the adiabatic efficiency of the ducted fan and is about 90 ~ 92%.

To further delineate which losses are and which losses are not included in the transport efficiency, Table 3 is provided. Also, no advantage was taken of the fact that the test was run at a low Reynolds number and one would expect a generally favorable effect in going to full size.

All of the configurations tested were run through the transport efficiency calculation procedure described above (see Appendix A for the description of this program). Although the primary emphasis of this analysis is placed on the more promising configurations

(taken to be those with transport efficiencies of 5 or greater), the other data was also used to provide either additional information or confirmation of the conclusions made. Of roughly 230 configurations evaluated, 15 of the higher ones were selected on this basis. Consequently, there is some possibility that interesting trends may have been missed, but these are not likely to influence vehicle design as they occur at lower transport efficiencies.

GENERAL RESULTS OF THE TESTING PROGRAMS

INTRODUCTION

The following sections report the general trends recognized from careful analysis of the test data. Each section describes the effect on vehicle performance produced by varying one of the major vehicle parameters, holding all others constant (or as nearly so as possible). Vehicle performance has been judged by the resultant values of transport efficiency and flying height. The transport efficiency provides an indication of the effectiveness of the particular configuration, and the flying height, or heave, provides a measure of the usefulness of the vehicle (a very efficient design which must fly so low that it runs into waves is actually a poor design). The final section discusses the effect of vehicle design upon the vehicle acceleration curve (T_{EX}/W). Where possible, a typical increment in performance is provided for a given increment in the parameter. In cases where the increment is not constant but varies regularly with other factors, the apparent variance is described, but no graphs predicting the effect of combinations of parametric changes are presented due to insufficient data. The final case is that of variance in the performance increment with no perceptably consistant relation to other parametrics. When this occurs, the effects are bracketed to hopefully cover the configuration of interest, and the data is presented in intermediate form.

Note that where dimensional results are given, they refer to the test model.

ASPECT RATIO

Analysis of the test data performed with respect to the wing aspect ratio reveals a very interesting pattern in the performance behavior. The results indicate that the transport efficiency of the model decreases as the aspect ratio is increased, reaching a minimum for an A of approximately one. Increases in A beyond this point produce higher transport efficiencies. The heave of the model generally decreases with increases in A. The aspect ratios investigated were 1/2, 3/4, 1, 1 1/2, and 2.

This analysis, due to insufficient data, is based primarily on configurations which do not display exceptionally good performance (defined by the arbitrary 5.0 transport efficiency cutoff), but rather are those showing average or above average performance and holding all vehicle parameters constant except aspect ratio. The specifications of one of these configurations are presented below.

$\delta_f = 40^o$

$\epsilon_f = 20^o$

$\alpha = 0^o$

W/S = 5.5

T/W = .21

A = 1/2, 3/4, 1, 1 1/2, 2

Other "spot checks" were made at several other model configurations to substantiate the conclusions. Although data sets were found which permitted a study of aspect ratio effects (one of which is presented in Table 4, corresponding to the previous specifications), even these cases do not compare identical configurations, as the fan densities and endplate heights sometimes vary. However, effects due to these factors are taken into account and the conclusions which are presented reflect corrected data.

Figure 8a shows the effect of aspect ratio upon transport efficiency. Conclusions based upon this and other data indicate that the wing of aspect ratio one is the least efficient and that higher or lower A's produce the best performance. But it should also be noted that the slope of the left-hand side of the curve is twice as great as that of the right, so that to obtain a given positive increment in η_T, it would be necessary to increase a high A (>1) twice the amount necessary for one which is low (A<1). This would suggest very good performance from an aircraft which uses only a small part of its span for power augmentation, such as a STOL aircraft might use.

The heave of the model demonstrated a slight decrease with greater aspect ratios. This decrease, shown in Figure 8b, is on the order of 0.1 - 1.5 inches (0.25 - 3.81 cm), the higher occuring at the A's below one. An interesting result is found by comparing the heave values to the length of the respective endplates. This comparison shows that when the model was tested with 5.5 inch (14.0 cm) endplates, the heave was such that the endplates were out of the water 3.6 - 2.8 inches (9.1 - 7.1 cm), highest for lowest A, while the 7.75 inch (19.68 cm) below the surface. No conclusions have been reached regarding this phenomenon.

ANGLE OF ATTACK

Evaluation of the data with respect to the effect produced by increasing the wing angle of attack, within the range of 0 - 4 degrees, reveals that the performance of the model is improved by decreasing α. Large increases in transport efficiency, with small decreases in heave, result when α is brought to zero. This conclusion is true for configurations having either high or low transport efficiencies.

Table 5 provides angle of attack data for promising configurations. This shows that if the angle of attack is increased two degrees, the transport efficiency is decreased from 13 to 78 percent, the largest reduction occuring for the higher aspect ratios and/or configurations

having very high η_T's at zero incidence. There is also less effect upon transport efficiency in going from 2 to 4 degrees than from 0 to 2 degrees.

The data also shows that the heave of the model increases as α is increased, as would be naturally expected. The magnitude of this increase was reasonably constant, varying between 6 - 12 percent. For all of the cases which were examined, the endplates were out of the water at zero incidence angle, thus the increase in heave increased this clearance (whereas if the endplates were submerged at $\alpha = 0$, the additional heave might be less, due to the sudden loss of pressurization when the endplates cleared the water). No relationship between other parameters and the magnitude of heave increase was determined.

FLAP ANGLE

The deflection angle of the trailing edge flap affects the vehicle's lift and drag characteristics, so naturally it would have a substantial effect upon its transport efficiency and heave values. An evaluation of the performance differential with respect to the flap angle has shown that, without exception, the transport efficiency rapidly decreases and the heave moderately increases when the flap angle is increased from 20 to 40 degrees. Both of these results are to be expected, though the drag increase, reflected through the η_T increment, is larger than expected.

Referring to Table 6, which presents heave and transport efficiency values for the configurations showing highest performance potential, it is seen that high transport efficiencies were obtained for both high and low δ_f. Analysis of all of the data shows convincingly that the transport efficiency decreases when δ_f is increased from 20^o. That there are test cases in which high transport efficiencies were obtained at high flap angles with no corresponding configurations of lower δ_f having higher η_T's than these is a result of an extrapolation problem in the data reduction computer program. Most of the configurations

which produce very high transport efficiencies have excess thrust curves which are both very high and very flat. When an extrapolation is made to determine the zero excess thrust velocity (trim speed), based upon the data, the velocity which is predicted is very high, often above 100 ft/sec (30.5 m/sec). The routine then attempts to extrapolate the thrust required at this speed using the data thrust curve, but usually a negative thrust results because of the high trim speed. Thus, no transport efficiencies could be determined for these cases, which actually show the most promise due to high excess thrust, although it would be expected that the excess thrust curve would begin to drop more sharply at a higher speed than tested and thus allow η_T to be calculated. Figures 6r - 6v are computer - generated plots which demonstrate the characteristics of these special cases. For the cases having high η_T for a low flap angle, the decrease in η_T produced by increasing the angle to 40^o ranged from 45 - 90%. The cause of this variation has not been established, but the cases having the highest transport efficiencies showed the greatest decreases.

Table 7 presents the heave results for some of the configurations, as well as the trim speeds. The information shown, as well as much of the remaining data, shows an interesting aspect of this study and this must be realized before interpreting the results. If the heave values for both flap angles are compared, for most of the cases it is seen that a higher heave exists for the lower angle, which contradicts the premise which has been made. This is explained, though, by also comparing the trim speeds, where it is seen that in many cases, the trim speed for the 20^o flap deflection is much less than that of the higher angle. This means that, since the heave curves are increasing within the trim speed velocity range (greater than 20 ft/sec), the higher velocity produces a higher heave extrapolation. Actually, as can be seen by studying Figures 6a - 6v , the effect of increasing the flap angle from 20 to 40 degrees is to shift the heave curve upward approximately 1.6 inches (4.06 cm). Thus, for the same velocity, this would be average heave increment for this increase in δ_f.

FAN ANGLE

A review of model performance with respect to the propulsor (fan) angle, ϵ_f, shows that the transport efficiency slightly decreases and heave is generally unaffected when ϵ_f is increased in five degree increments. The configurations having low (15^o) or high (40^o) fan angles did show heave values which were lower than the others (between these extremes). Due to a limited run matrix and some problems with data taken for varying ϵ_f, only five data points (one configuration at 5 ϵ_f's) are available for analysis.

Table 8 presents the available data and Figure 9a shows the transport efficiency data graphically. That η_T decreases with increases in ϵ_f is not only a conclusion drawn from both this (scarce) data and by intuition, but also has been shown in previous tests and through theoretical consideration. Figure 9a shows that the effect of ϵ_f on η_T is rather small, and in this respect additional data would be useful. From momentum considerations of the PAR phenomenon, it was expected that a larger decrease in η_T would be experienced. Since there is data for only one configuration, however, no conclusive results regarding the magnitude of the transport efficiency difference is possible.

The results of the model heave, shown in Figure 9b, indicate a behavior which also was not expected. It is seen that, aside from lower heaves at the 15^o and 40^o boundary points, the height of the model remains constant despite changes in ϵ_f. That the heave would decrease for high fan angles would be expected, since the flow angle is such that it is not greatly power augmenting the lift. The same argument may be used for very low fan angles, as much of the flow from the fans would not pass under the wing. Geometric consideration, however, shows that a fan angle greater than 5^o will direct the entire flow from the fan to beneath the wing, so that this is not the reason for a lower heave of 15^o. It is possible that error exists at this data point, and, since there is no evidence to either support or rebut this, it is assumed that no cause exists for the heave at 15^o to be discontinuous with those at higher angles (but below 40^o).

WING LOADING

When the wing loading, W/S, of a power augmented ram WIG is increased for an otherwise constant configuration, the resultant performance increment is highly variable. Due to coupling with apparently many vehicle parameters, primarily aspect ratio, generalized conclusions cannot be made. When analysis is made of those configurations showing the most promising performance ($\eta_T \geq 5.0$), it is found that 10 of 15 cases have wing loading of 5.5 lb per sq foot (26.85 kg per sq meter) or greater, so that one may say that higher wing loadings offer the best chance of producing a high performance WIG.

Referring to Table 9, which presents the results for the most favorable configurations, it can be seen that no obvious behavior pattern exists within the data. Comparing the W/S-induced transport efficiency changes for various configurations shows that generally the efficiency increases for higher wing loadings. It is seen that there is a strong dependence upon aspect ratio, with angle of attack and flap angle causing lesser, but often considerable, influence. Table 10 lists the wing loading ranges tested for several aspect ratios and the corresponding ranges of percentage change in η_T. Primarily, the differences in the transport efficiency improvement comes from changing the flap angle, angle of attack, fan angle, and thrust-weight ratio of the model. Referring to the section, dealing with aspect ratio influence, it is seen that the variation in transport efficiency increment due to changing aspect ratio demonstrates the same behavior as that of varying A alone, shown in Figure 10. From this realization, it may be concluded that wing loading produces variable influence on transport efficiency and that the ranges demonstrated through the testing program may be confidently used for parametric analysis of an aircraft (for the respective aspect ratios).

The results for heave are much the same as those for transport efficiency. When the ranges of h_w are plotted as is η_T, the appearance

of the curve is the same, thus no figure has been included.

THRUST-WEIGHT RATIO

Evaluation has shown that when the thrust-weight ratio, T/W, of an efficient PAR WIG aircraft ($\eta_T > 5.0$) is increased, the performance which results is significantly improved, both in efficiency and operating height. The T/W range investigated for the promising configurations is .19 - .35. The results also show that if the configuration displays poor performance, higher T/W causes a further loss in transport efficiency.

The results of this analysis indicate the importance of proper parametric matching, as there is strong coupling between the many configurational aspects of the vehicle. For many of the model configurations which produced high transport efficiencies at low T/W, η_T was increased three times the percentage increase in T/W. This, however, is not true for all of the cases, as some configurations experienced decreases of the order of the T/W increase. Two sample cases of both of these results are shown in Table 10, though it is emphasized that 5 of 7 high η_T configurations demonstrated η_T increases. All of the low efficiency configurations had lower transport efficiencies at the higher thrust weight ratios. No relationship has been found to predict whether the transport efficiency of a high performance PAR WIG increases or decreases with higher T/W.

As would be expected, the heave of the model increases when the thrust-weight ratio is increased. This is true whether the configuration has a high or low η_T. In most of the data, this increase was 1/2 of the

percentage increase in T/W, so this may be used as a rule of thumb.

FAN DENSITY

When the number of power-augmenting propulsors per unit span, the fan density $n_{f/b}$, is increased, the aircraft's performance also increases. This is of course true only up to some limiting value, but the testing programs did not explore this maximum. The fan densities examined were between 0.5 and 1.0 fans per foot (.15 - .30 fans per meter). The most promising configurations, with the exception of two, all had a fan density of 1.0, which strongly indicates that this is a critical aspect of vehicle design.

Table 11 presents a partial listing of the data used for this analysis. When $n_{f/b}$ is increased within the previously mentioned limits, it is found that the transport efficiency increases by 28 percent, with reasonable constancy despite the variance of other parameters. The heave, however, shows a high degree of coupling with the other parameters and demonstrated a range of heave decrease of 0 - 50%. The coupling behavior is such that decreasing the thrust-weight ratio and increasing the flap and wing incidence angles cause the largest changes in h_w. This can be seen in Table 12, a comparison of the best and worst performing configurations which were tested. It should be noted that the only configuration for which the fan density was changed was that of aspect ratio one, thus no judgement can be made on the aspect ratio effect on these conclusions. Provided that the fans are evenly spaced across the span, it is reasonable to assume that no variation would occur for different aspect ratios.

COMPARISON OF ROUGH AND CALM WATER PERFORMANCE

This study is made to determine the degree of performance lost, if any, when operating the PAR WIG model in Sea State 5 conditions. Provided that the flying height is satisfactory, performance could be lost due to the variation in the volume below the wing and changes in the trailing edge gap, not because of contact with the waves. However,

the results show that operation in waves does not produce results much different from those under calm conditions and, therefore the results from calm water tests (which greatly outnumber those in Sea States, due to the number of runs necessary to meet the required wave encounters for irregular wave spectra) are directly applicable to predict performance under actual conditions.

Table 13 presents a sample of the data which was reviewed. It should be understood that no conclusion has been drawn regarding whether the transport efficiency increases or decreases as the Sea State increases (in fact, both bases occur in the data), but more importantly is shown that the efficiency can remain high in spite of high Sea State conditions. The same is true of heave, being only marginally effected by the presence of waves. These conclusions are extremely important, for they prove that PAR WIG's are capable of significant performance under realistic operating conditions, not simply under ideal (and rare) ones.

PARAMETRIC EFFECTS UPON ACCELERATION

This is a brief synopsis of the acceleration characteristics of various PAR WIG configurations. It is intended only to give some insight into the effects of the various configurations upon acceleration, and is not a complete investigation as was accomplished for heave and transport efficiency.

Figures 11 to 15 are provided as examples of acceleration curves of the various parametric configurations. These configurations are of two aspect ratios; the T/W, W/S, and δ_f comparisons use data of aspect ratio one, and the α and C_f comparisons are of aspect ratio two. The following comments are observations based on these figures.

- α - Figure 11 shows that the acceleration is higher for the model at zero angle of attack (approximately .02g higher), which is the same conclusion reached for the η_T analysis.
- δ_f - Figure 12 indicates that a lower flap deflection angle yields a higher acceleration (approximately .05g for the 15^o difference), also the same conclusion as found for η_T.

Θ_f - Figure 13 shows that a fan angle of 25^o provides the highest acceleration, slightly higher than that of the 30^o configuration.

W/S - Figure 14 shows that the acceleration curve is almost constant for wing loadings of 4.3 and 5.5 lb per sq ft (21.0 and 26.8 kg m^2).

T/W - Figure 15 shows the result that is obviously expected, that higher thrust-weight ratios produce higher acceleration curves.

Finally, it should be noted that in all cases, the curves are practically parallel and all peak at the same speed.

DISCUSSION AND CONCLUSIONS

In this section, the results which have just been presented will be discussed in an effort to determine their significance and shortcomings. This discussion will not only seek to provide reasonable (but brief) explanations for these results, as well as their agreement with theory, but also to compare these with the effect of similar wing geometric changes in a conventional aircraft to observe any radical differences. The format of these comments is the same as that of the preceeding section; i.e. in subsections which individually refer to each of the eight parameters.

ASPECT RATIO - One of the fundamentals of aircraft design is the decrease in induced drag with higher aspect ratios, due to a decrease in the area of the airfoil which is affected by wing downwash. With a WIG vehicle, the induced drag is also decreased by its ground effect flight and end plates. For aspect ratios of one or greater, the results show that the classical aspect ratio effect is produced, for the transport efficiency increases with A. There is , however, no fundamental explanation for the decrease in η_T between aspect ratios 1/2 and 1. It is possible that because of the short span of the low aspect ratio wings, the flow beneath the wing may be more homogeneous then that of higher A configurations. If this is so, the pressure distribution beneath the wing would be more

consistent and the power augmentation would be more efficiently applied, overcoming the increased drag from the lower A wing. Further evidence that this may be what is occuring can be found by referring to the aspect ratio 3/4 and 1 configurations. The transport efficiency for the 3/4 case is greater than that of the A = 1 case, even though the A is larger and fan density higher for an aspect ratio of one. This means that some mechanism is responsible for overcoming the increased induced drag due to lower A and the decreased power augmentation due to lower $\eta_{f/b}$ to produce a higher η_T. It is obvious that the aspect ratio problem must be further studied.

ANGLE OF ATTACK - Increasing the angle of attack of a PAR WIG, as with any wing section, increases the lift and drag of the wing. With the WIG, however, the trailing edge gap is also reduced (for a given wing height), thereby reducing both pressure recovery and drag. The results have shown that η_T rapidly decreases with increases in the angle of attack. The only simple explanation which can be offered at this time is that the higher angle increases the spillage of the flow at the leading edge of the wing and leakage of air under the leading edge of the endplate (due to reduced draft), therefore reducing the augmentation.

FLAP ANGLE - When the trailing edge flap of a wing is deflected some positive angle, the increased wing camber produces large increases in both lift and drag. With a WIG aircraft, this flap deflection also decreases the trailing edge gap, which in Reference 3 has been shown to increase lift and reduce drag. It was therefore expected that there would not be much decrease in η_T when the flap deflection was increased, as the drag increase should be minimal. The results, however, have shown that increasing the flap deflection from 20 to 40 degrees produces a large decrease in η_T. One of the reasons for this (if not the sole reason) was presented during the flap discussion in the model description section. Due to the way in which the flap was mounted during construction, a large gap exists at the upper surface of the wing when the flap is deflected, the width of the gap increasing with flap angle. Thus, since the size of the gap causes premature flow separation and its associated

drag rise, large flap deflections produce much more drag than would a typical flap installation. Also, because of the increased excess thrust that a proper flap would produce, the acceleration of the vehicle would be correspondingly higher. The heave shown may be considered typical of the increased lift which the flap provides.

FAN ANGLE - The results show that η_T only slightly decreases when θ_f, is increased. PAR theory has not yet been developed for fans at various angles and locations, so no results are available to predict its effect on transport efficiency. From geometric considerations, one would expect considerable loss in transport efficiency due to high fan angles. Even though the transport efficiency losses which were experienced in the tests were small in magnitude, it should be noted that the transport efficiency, as defined in this report, includes losses in jet velocity associated with fan deflection.

WING LOADING - In conventional aircraft design, the wing loading is an important parameter to optimize, for it increases the structural efficiency but decreases take-off and landing performance. The data does not give a clear indication of the performance gained by increasing W/S. The coupling of this factor with the other wing geometric parameters indicates that the greatest improvement in η_T due to increasing W/S is produced at those configurations which are most nearly performance-optimized. The effects of each geometric parameter is apparently amplified by the higher loading of the wing surface.

THRUST-WEIGHT RATIO - Earlier static evaluations, DTNSRDC internal working papers, ASED TM 16-76-76 (June 1976), have shown that high static augmentation ratios (L/T approaching 6.0) are possible. The results show this to be true for the model, provided that the configuration is one having a good performance potential. These cases have shown large increases in η_T when T/W is increased. The

primary reason for this is due to the higher excess thrust curve (from the higher thrust level). This additional excess thrust produces a higher trim speed, and this speed goes directly into the numerator of the η_T equation, thus increasing η_T the same amount as V_{TRIM}. This report will not present speculations on any other causes.

FAN DENSITY - The results have shown that the best performance occurs for a fan density of one, but this was the highest tested so that the maximum is not known. References 1 and 2 indicate that, depending upon the thrust coefficient and the pressure recovery which is desired, the fan diameter to wing height ratio should be approximately 35 to 70 percent. This of course refers to a two-dimensional wing and assumes a two-dimensional jet, thus it would also rel-te the fan (jet) area to the wing inlet area. For given fan area, wing geometry, wing height, and pressure recovery (the last adjusted by the trailing edge gap), the number of fans required to meet this ratio may be computed. At the conditions of the test model, the number of fans required is at least one per foot of span, which gives a ratio of 35% for a one foot wing height. It should also be noted that the distance of the propulsor ahead of the wing would have a performance effect, in that it determines the increase of the jet area, caused by flow entrainment, upon entering the below-wing volume. This distance was not investigated in this program.

PERFORMANCE IN WAVES - The conclusion that waves up to Sea State 5 do not significantly affect the performance aspects dealt with in this study is a very meaningful result. The performance in waves is roughly the same as that over equivalent calm water located 1/4 the significant wave height above the mean sea level.

RECOMMENDATIONS

On the basis of the parametric analyses which have been presented, a prediction may be made for the optimum configuration of a PAR WIG

aircraft. The optimum configuration, for the purposes of this study, is defined as one which operates at a height sufficient to clear all waves of its maximum operational Sea State, with the maximum transport efficiency. As a result of these criteria, the following vehicles configuration is offered which indicates the greatest potential for achiefing these goals. These are presented in Table 14 along with the specifications of the configuration having the highest transport efficiency of the data set. Due to the nature of the parametric investigation and that no maximum value was encountered, specific values are not given for the aspect ratio, thrust-weight ratio, wing loading, and fan density. However, the results have established the best value of those tested, so that this is used as the start of the possible range. The results presented in this report should be sufficient to substantially reduce the test matrix necessary for a complete exploration of the region of the parametric space of major interest. The primary focus of further research should be the aspect ratio, thrust-weight, and propulsor location/geometry effects upon the vehicle performance. Such investigation would be invaluable for enabling accurate choices of configurations for PAR WIG designs.

REFERENCES

1. Gallington, W.W., "Sudden Deceleration of a Free Set at the Entrance of a Channel", DTNSRDC Departmental Report ASED 350 (Jan 1976).

2. Gallington, R.W. and H.R. Chaplin, "Theory of Power Augmented Ram Lift at Zero Forward Speed", DTNSRDC Departmental Report ASED 365 (Feb 1976).

3. Papadales, B.S., "An Evaluation of a Two-Dimensional Power Augmented Wing in Ground Effect Model Under Static and Dynamic Freestream Conditions", DTNSRDC Departmental Report ASED 353 (June 1976).

APPENDIX A

DESCRIPTION OF DATA REDUCTION/PLOTTING COMPUTER PROGRAM

The data which was generated during the testing programs was reduced using a Fortran IV computer program which put this information in a more useable form. This program was used in two ways. It was originally developed to prepare plots of the actual and extrapolated data, as well as list calculated derivatives of the data. It was found, however, that a relatively large amount of computer time was required to generate a plot for each data group, and additional expense was required to actually obtain plots on a Calcomp 763 plotter. Therefore, the program was slightly modified so that the data could first be manipulated within the program and only a few results printed out, with no plots produced. From these results, the most promising configurations were rerun, this time having the program generate the plots. This program was designed for use on DTNSRDC's CDC 6700 computer with the aid of the DISSPLA plotting package (developed commercially by Integrated Software Systems Corp.)

Given the model geometry and data (V, h_w, D, T) for each data group, the program was developed to extrapolate the model's trim speed, thrust drag and heave at trim, and to calculate the transport efficiency, acceleration, and wing C_L. The extrapolation which is used is a conventional cubic spline curve fit which only makes use of the last three data points (i.e. the highest three velocities tested). Knowing the thrust and drag at each point, the excess thrust (hence the acceleration $\frac{T_{EX}}{W}$) is found. The trim speed is found by extrapolating the $V\text{-}T_{EX}$ curve to zero excess thrust. Using this trim speed, the heave, thrust, and drag at this speed are extrapolated in the same manner. With this information, the transport efficiency lift coefficients; the actual C_L of the model at the particular model configuration, the two-dimensional C_L of the airfoil used, and the two-dimensional C_L with the flap deflection considered. This information, along with other necessary data of the configuration, is provided on the plot for each data case which indicated performance potential.

TABLE 1a - MODEL CONFIGURATIONS AND CONDITIONS TESTED (OF INTEREST)

DURING TESTING PROGRAM 1[1,2]

A	$n_{f/b}$, fan/ft (fan/m)	h_{EP}, in (cm)	α, deg	δ_f, deg	W/S, lb/ft^2 (kg/m^2)	V ft/sec (m/sec)
1/2	1 (.3)	7.75 (19.68)	0, 2, 4	20, 25, 40	3.0, 4.3, 5.5 (14.6, 21.0, 26.8)	0 45.0 (0 13.7)
1	1 (.3)	7.75 (19.68)	0	40	5.5 (26.8)	0 35.0 (0 10.7)
3/4	2/3 (.2)	5.50 (13.97)	0, 2	20, 25, 40	4.3, 6.0, 7.6 (21.0, 29.3, 37.1)	0 35.0 (0 10.7)
1	1 (.3)	7.75 (19.68)	0, 2	20, 40	4.3, 5.5 (21.0, 26.8)	0 35.0 (0 10.7)
1	1/2 (.15)	5.50 (13.97)	0, 2	20, 25, 40	4.3, 5.5 (21.0, 26.8)	0 35.0 (0 10.7)
1	1/2 (.15)	7.75 (19.68)	0, 2	20, 40	5.5 (26.8)	0 35.0 (0 10.7)
1 1/2	2/3 (.2)	5.5 (13.97)	0, 2	20, 40	4.3, 6.0 (21.0, 29.3)	0 35.0 (0 10.7)

[1] All runs were made in calm conditions

[2] Only the first series (A = 1/2) varied θ_f (10^o, 15^o, 20^o)

TABLE 1b - MODEL CONFIGURATIONS AND CONDITIONS TESTED (OF INTEREST) DURING TESTING PROGRAM 2[1,2]

A	ENDPLATE DESIGN	α, deg	δ_f, deg	θ_f, deg	SEA STATE	V, ft/sec (m/sec)
1	BASIC	0	40	20	4, 5	0 35 (0 13.7)
1	FLEXIBLE	0	40	20	0, 5	0 35 (0 13.7)
1	METAL	0	40	15-40	0, 5	0 35 (0 13.7)
1	BASIC	2	40	20	0	0 35 (0 13.7)
2	METAL	0	40	20	0	0 35 (0 13.7)
2	SHALLOW METAL	0	40	20	0	0 35 (0 13.7)

[1] All configurations had rigid flaps

[2] Wing loading was 5.5 lb/ft^2 (26.8 kg/m^2)

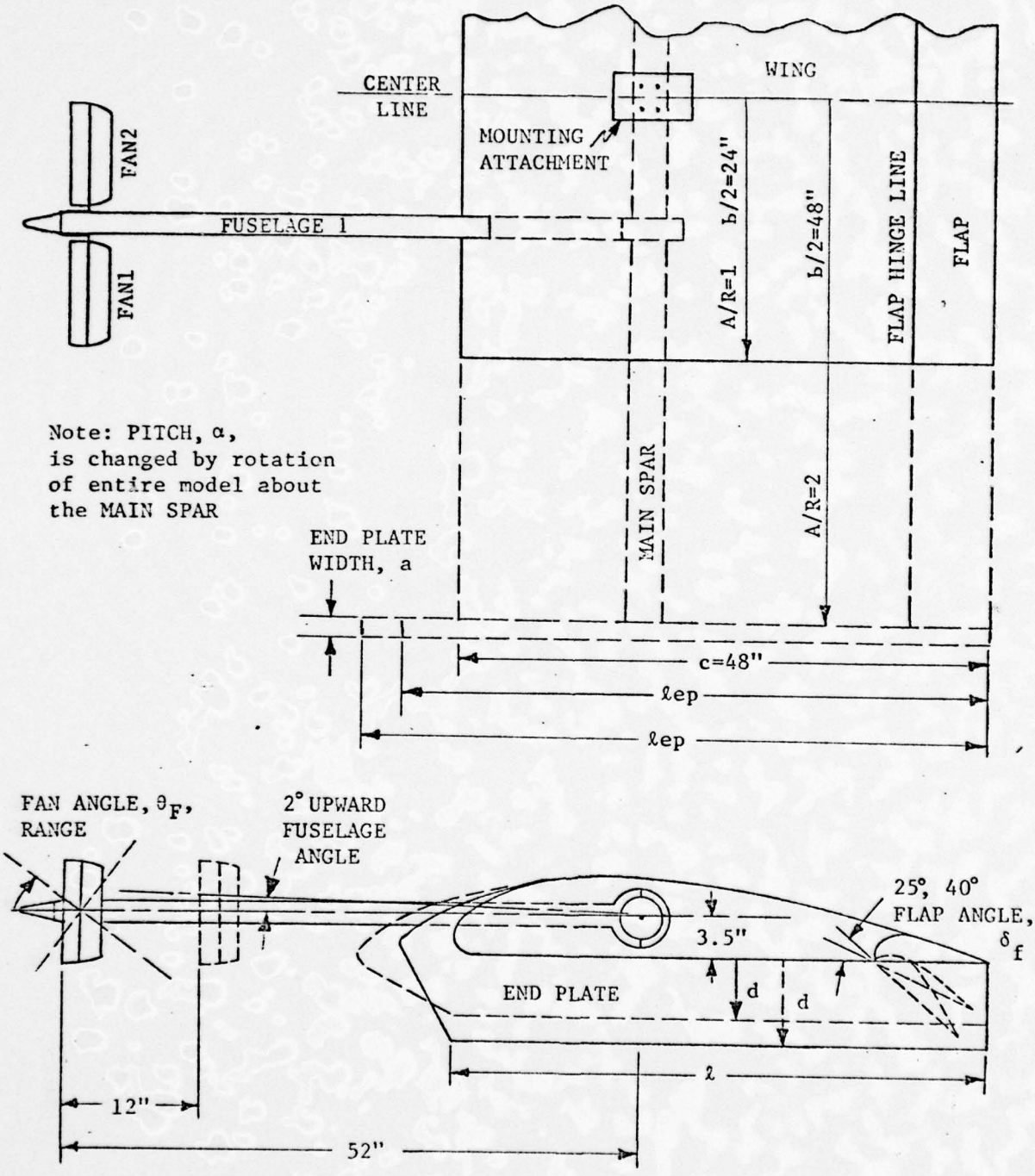


Figure 1 - PAR WIG Model General Arrangement

$b_1 = 3$ ft $b_2 = 2$ ft $b_3 = 1$ ft

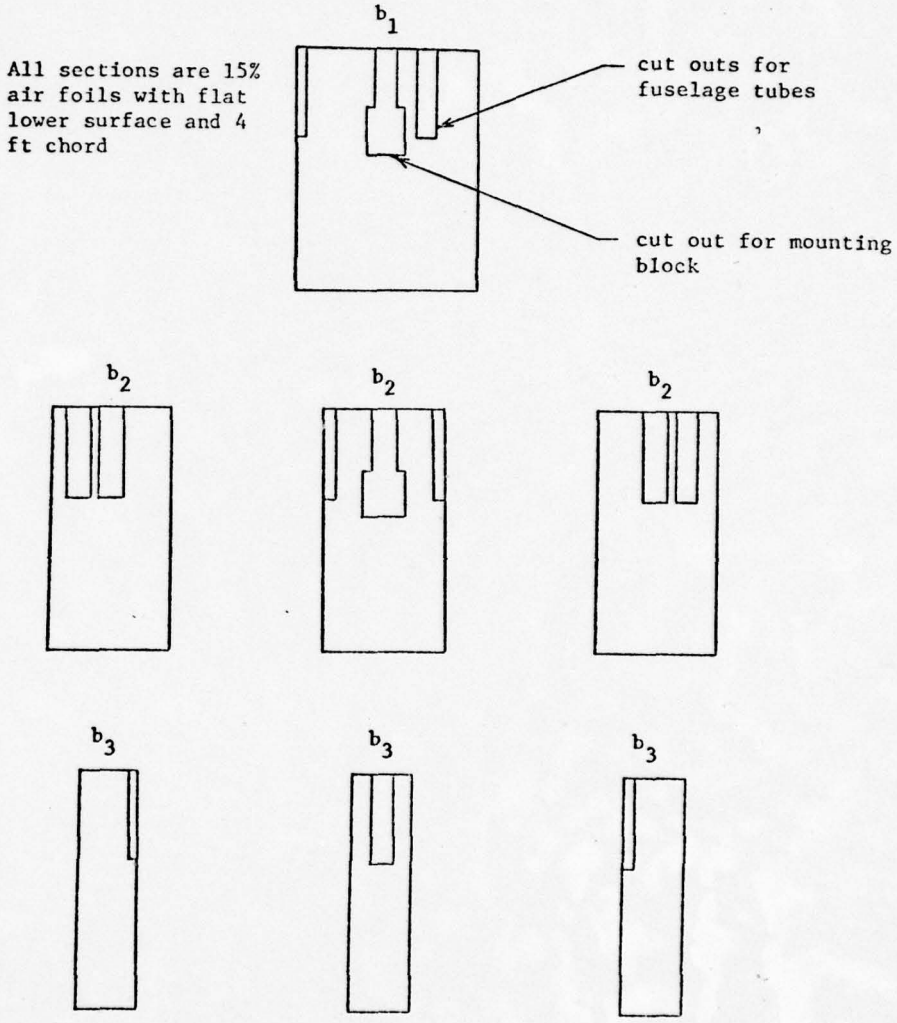


Figure 2 - Various Wing Planform Sections Available

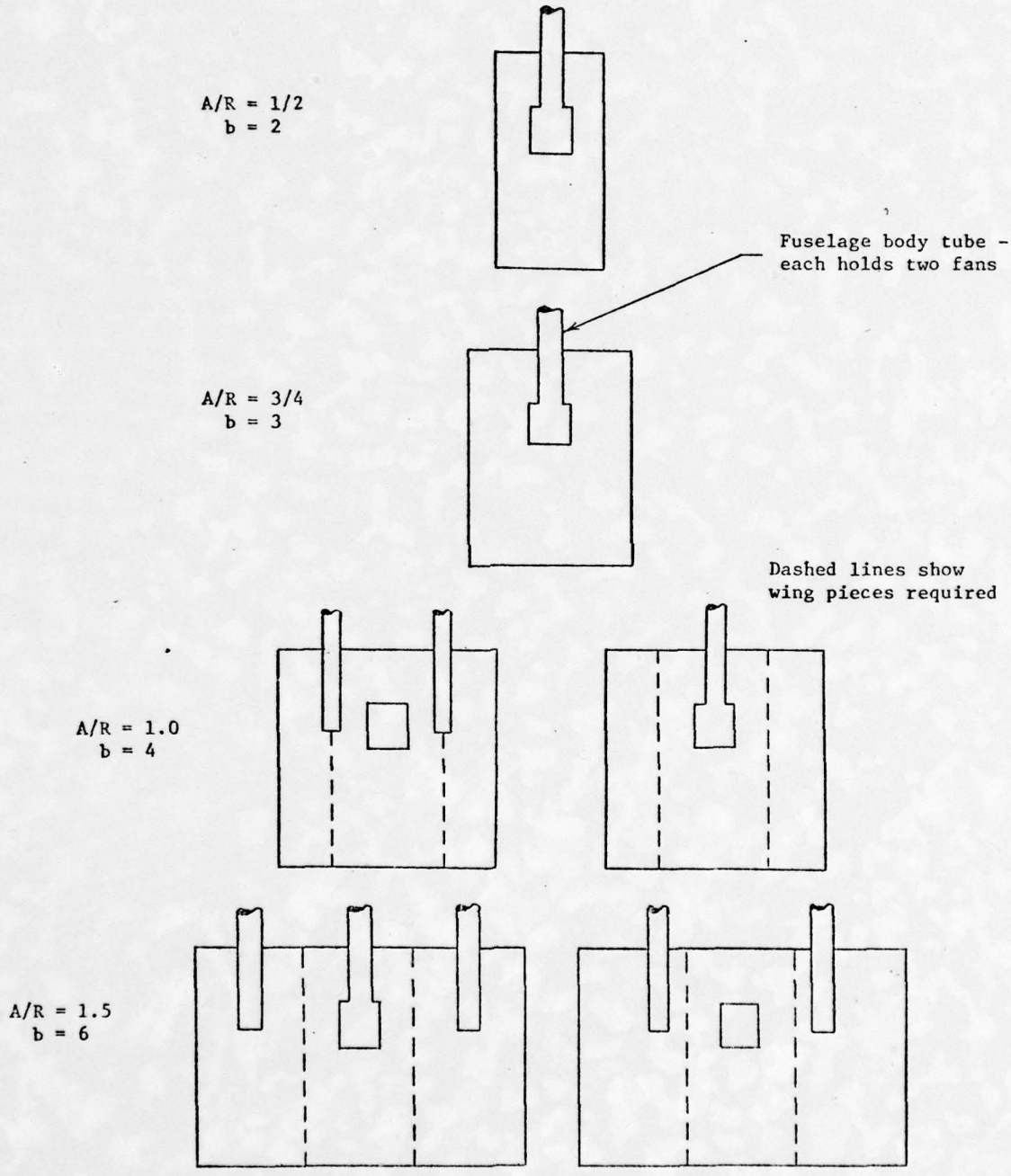


Figure 3 - Configurations Available for Testing, Planform View

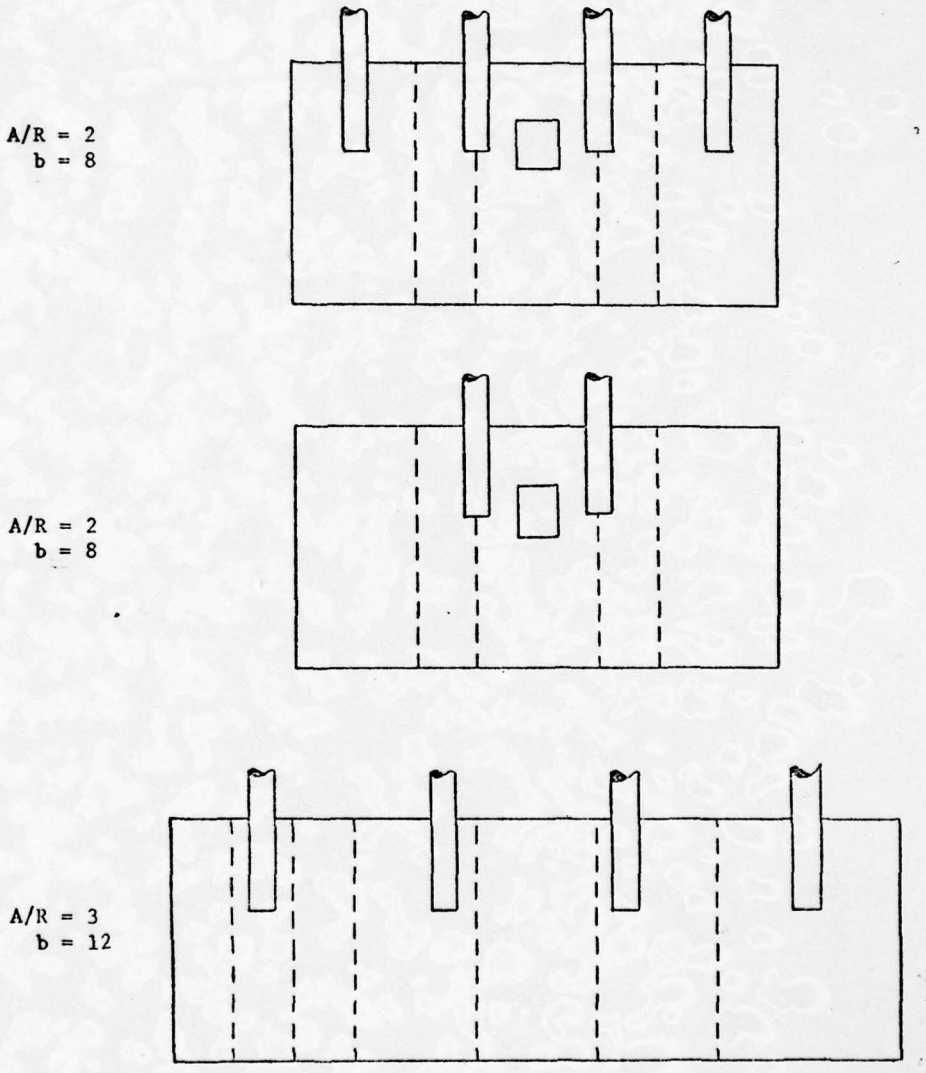
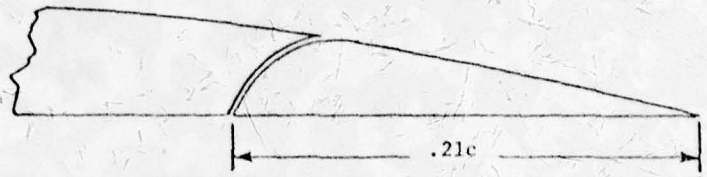
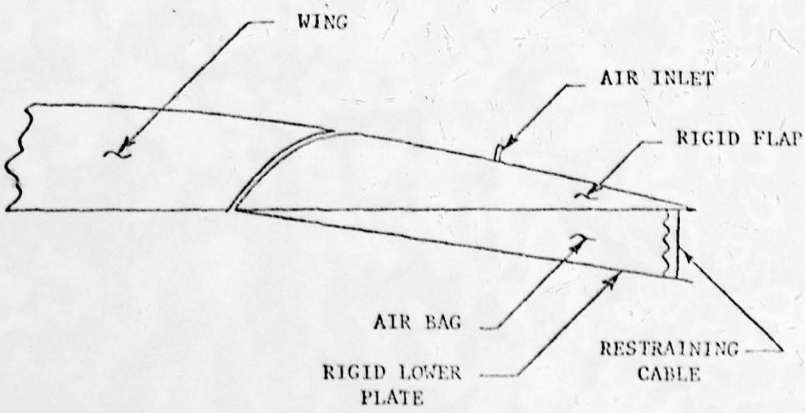


Figure 3 - (Continued) - Configurations Available for Testing, Planform View



RIGID FLAP



FLEXIELE FLAP

Figure 4 - Model Flap Configurations

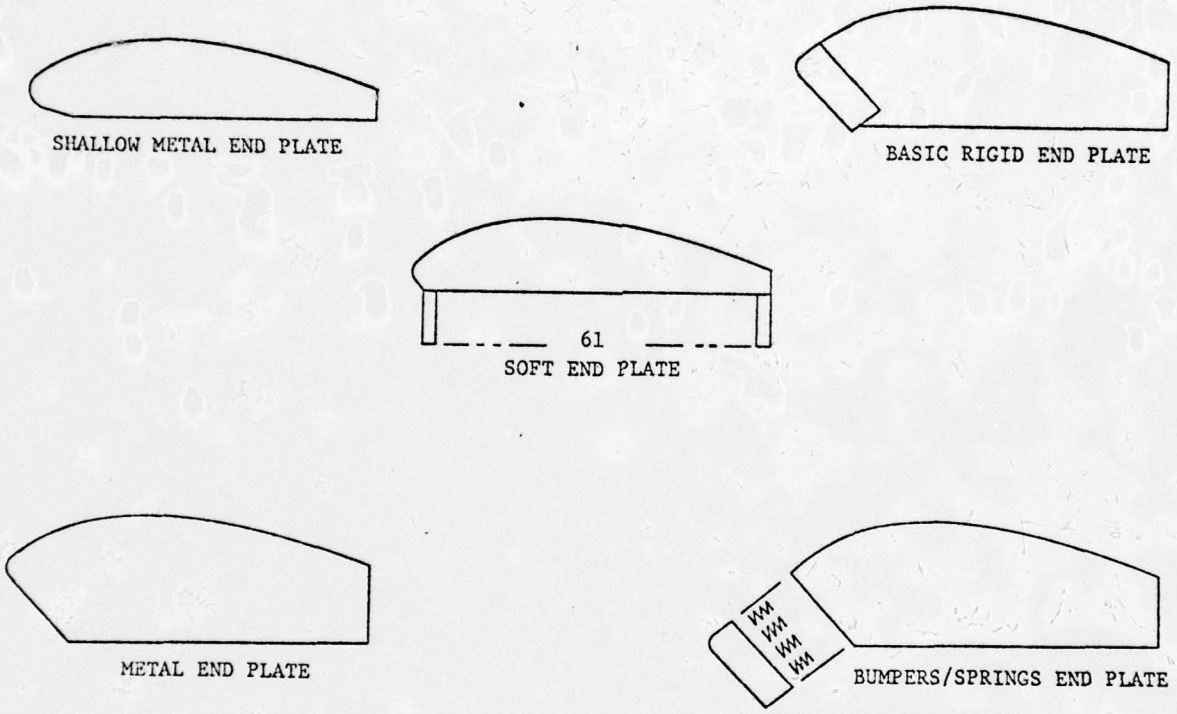


Figure 5 - Model End Plate Configurations

TABLE 2 - PAR WIG MODEL INFORMATION

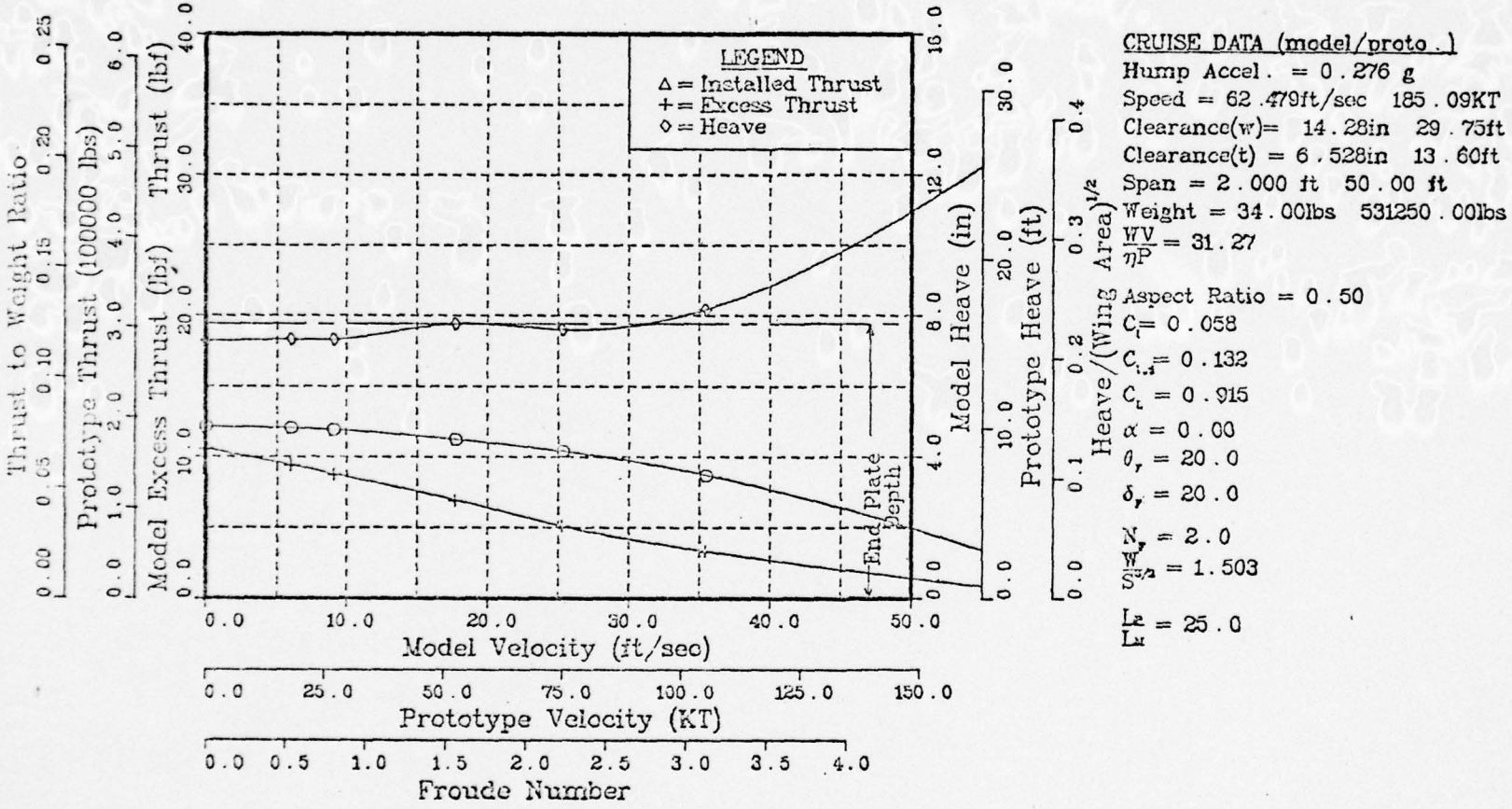
	FULL SCALE	1/30-SCALE
WING		
Airfoil Section	Flat-Bottom NACA 0015	
Chord, c	120 feet	48 inches
Span, b A/R = 1	120 feet	48 inches
Span, b A/R = 2	240 feet	96 inches
Taper Ratio	1	1
Thickness Ratio	0.15	0.15
RIGID FLAP		
Span A/R = 1		48 inches
Span A/R = 2		96 inches
Hinge Line		0.79c
Angles		25, 40 degrees
FLEXIBLE FLAP		
Span A/R = 1		48 inches
Hinge Line		0.79c
Fixed Portion Angle		20 degrees
Flexible Portion Angle		20 degrees
Air Pressure Motor		
Manufacturer		ROTRON INC.
Model Number		367JS
Diameter		2.12 inches
Number used		1
Maximum Output		59 $feet^3$ per minute
Pressure Range		0-16 pounds per $foot^2$
PROPULSOR FAN		
Manufacturer		TECH DEV., INC.
Model Number		TD-492
Diameter, D_F		8 inches
Maximum Thrust		37 pounds
Angle Range, θ_F		15-40 degrees
Number Used		4

TABLE 2 - (Continued)

	FULL SCALE	1/30-SCALE
NACELLE		
Maximum Diameter		10 inches
Length		4.5 inches
Number Used		4
FUSELAGE		
Length		49 inches
Width		2 inches
Height		2 inches
Angle, above mean waterline		2 degrees
Number Used		2
BASIC END PLATE		
Maximum Length, ℓ_{ep}		58 inches
Bottom Length, ℓ		43 inches
Width, a		1.27 inches
Depth Below Wing Bottom		7.12 inches
Deadrise Angle		60 degrees
Forebody Planing Surface Length		16.2 inches
Forebody Planing Surface Angle, above mean waterline		21.8 degrees
BUMPERS/SPRINGS END PLATE (BASIC END PLATE PLUS ENERGY ABSORBING FOREBODY)		
Number Springs Used		2, 4
Energy Absorbtion, per spring	26, 54, 78, 102	pounds per inch
FLEXIBLE END PLATE		
Maximum Length, ℓ_{ep}		48 inches
Bottom Length, ℓ		46 inches
Width, a		2.25 inches
Depth Below Wing Bottom		6.89 inches
Deadrise Angle		5.5 degrees
Forebody Planing Surface Length		5 inches
Forebody Planing Surface Engle, above mean waterline		85 degrees

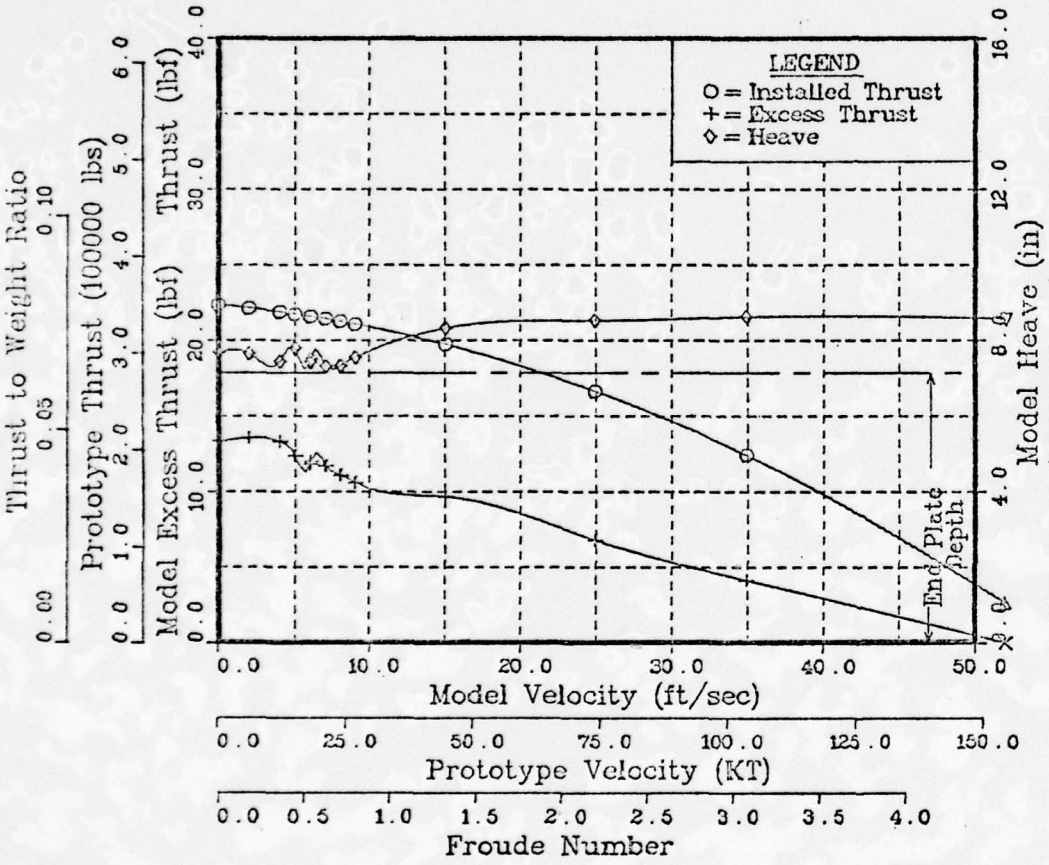
TABLE 2 - (Concluded)

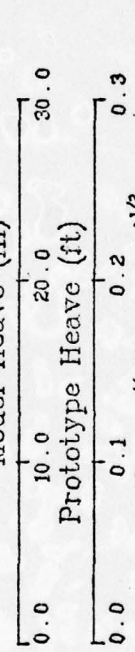
	1/30-SCALE
Flexible Finger Material	0.009 inch Nylon, Neoprene Impregnated
Flexible Finger Number	61
Flexible Finger Pressure Range	0 - 1 pounds per inch^2
METAL END PLATE	
Maximum Length, ℓ_{ep}	53 inches
Bottom Length, ℓ	48 inches
Width, a	0.25 inches
Depth Below Wing Bottom	7.75 inches
Deadrise Angle	0 degrees
Forebody Planing Surface Length	8.7 inches
Forebody Planing Surface Angle, above mean waterline	30 degrees
SHALLOW METAL END PLATE	
Maximum Length, ℓ_{ep}	56.75 inches
Bottom Length, ℓ	48 inches
Width, a	0.25 inches
Depth Below Wing Bottom	5.50 inches
Deadrise Angle	71.5 degrees
Forebody Planing Surface Length	9.2 inches
Forebody Planing Surface Angle, above mean waterline	18.75 degrees



CRUISE DATA (model/proto.)
Hump Accel. = 0.276 g
Speed = 62.479ft/sec 185.09KT
Clearance(w)= 14.28in 29.75ft
Clearance(t) = 6.528in 13.60ft
Span = 2.000 ft 50.00 ft
Weight = 34.00lbs 531250.00lbs
$\frac{WV}{\eta P}$ = 31.27
Aspect Ratio = 0.50
C_T = 0.058
$C_{T_{max}}$ = 0.132
C_L = 0.915
α = 0.00
θ_f = 20.0
δ_f = 20.0
N_p = 2.0
S_{wp} = 1.503
$\frac{L_E}{L_H}$ = 25.0

Figure 6a - Computer-Generated Plots of the Test Results for the Highest - η_T Cases





CRUISE DATA (model/proto.)

Hump Accel. = 0.155 g

Speed = 51.988ft/sec 154.02KT

Clearance(w)= 8.553in 17.82ft

Clearance(t) = 1.433in 2.986ft

Span = 4.000 ft 100.0 ft

Weight = 87.50lbs 1367188.00lbs

$\frac{WV}{\eta P}$ = 29.17

Aspect Ratio = 1.00

C_L = 0.111

C_{L_T} = 0.330

C_L = 1.700

α = 0.00

θ_T = 20.0

δ_T = 40.0

N_T = 4.0

$S_{3/2}$ = 1.367

$\frac{L_a}{L_w}$ = 25.0

Figure 6b - Computer-Generated Plots of the Test Results for the Highest - η_T Cases

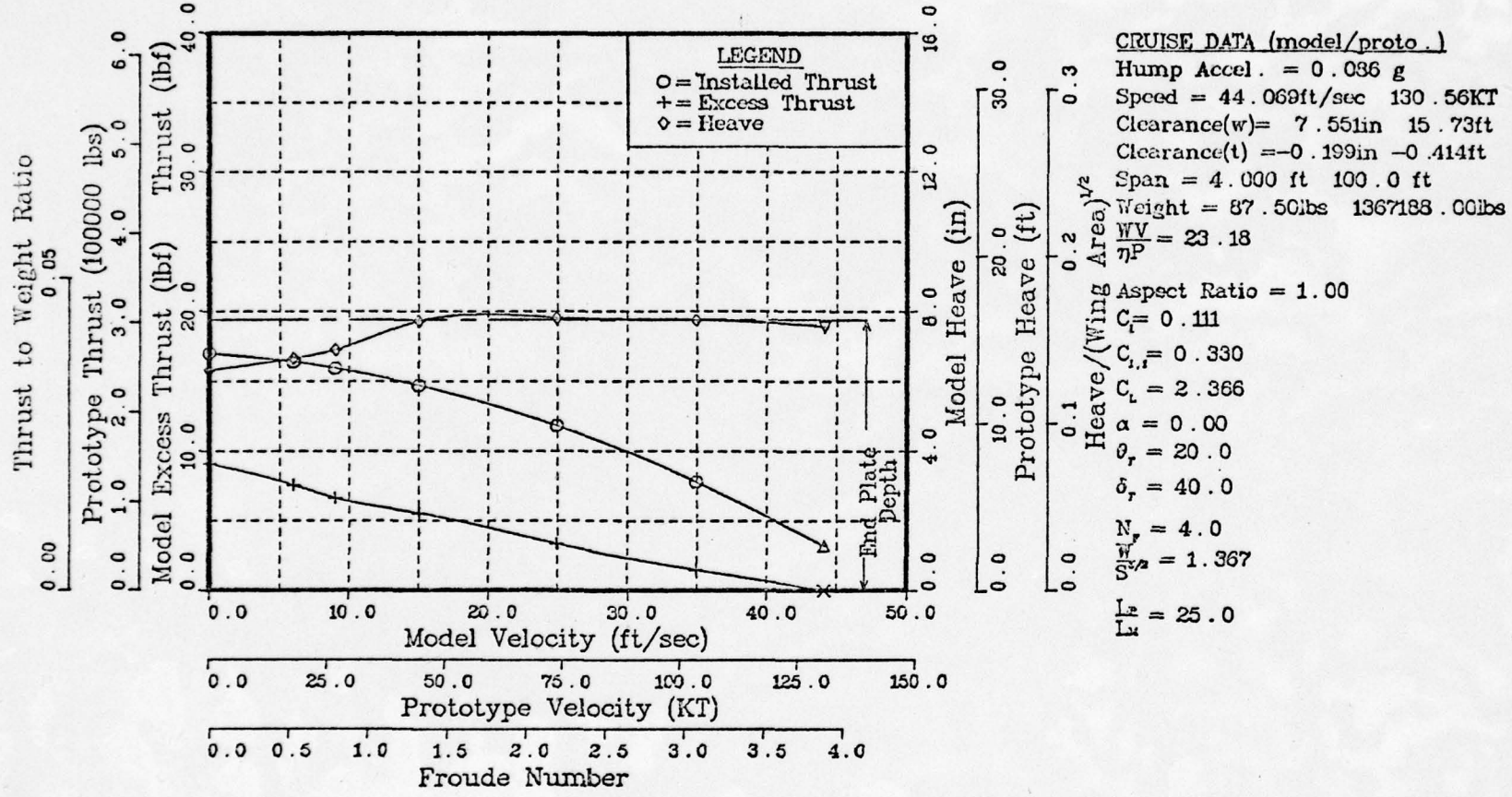
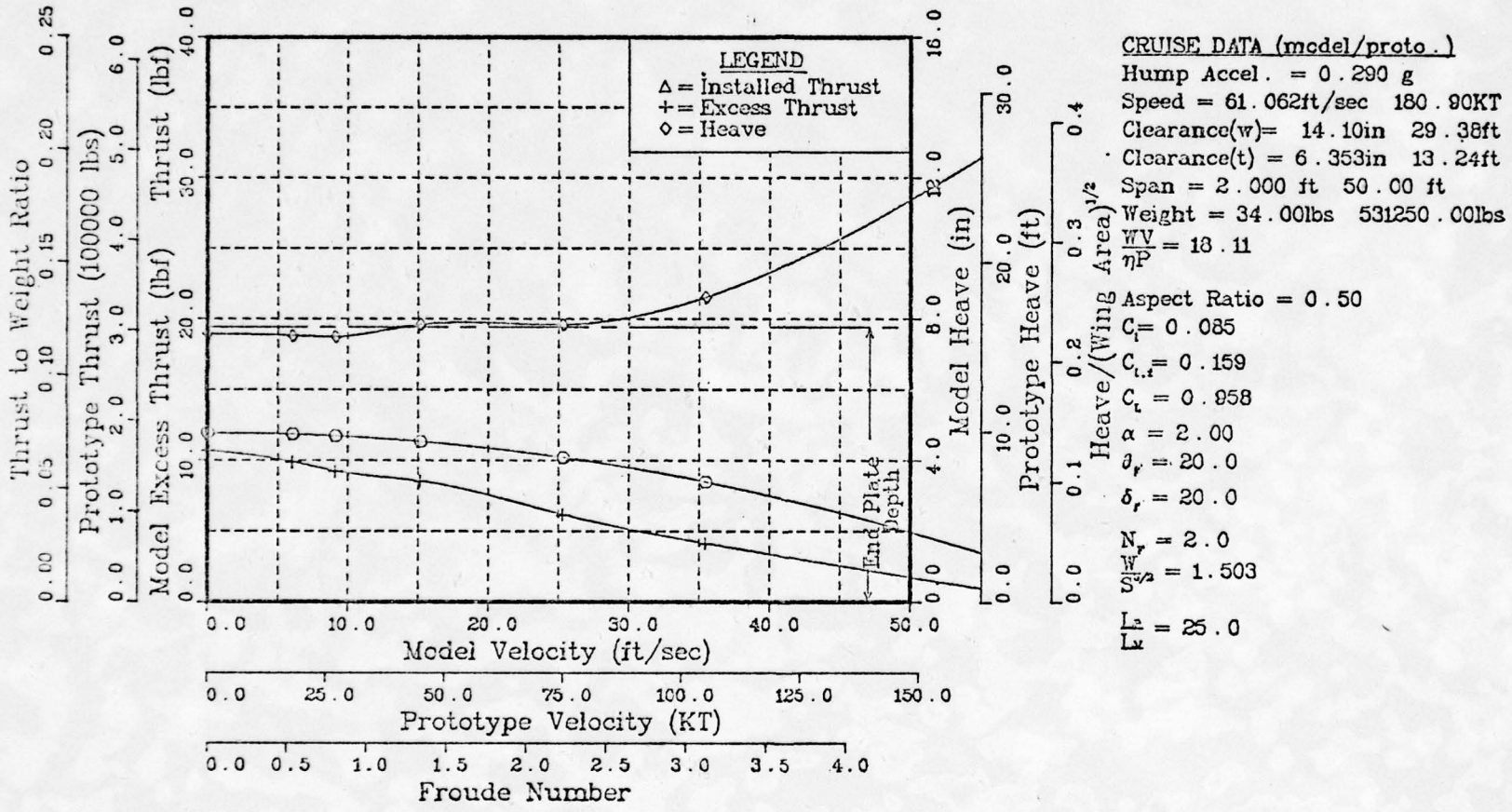


Figure 6c - Computer-Generated Plots of the Test Results for the Highest - η_T Cases



CRUISE DATA (model/proto.)

Hump Accel. = 0.290 g

Speed = 61.062ft/sec 180.90KT

Clearance(w)= 14.10in 29.38ft

Clearance(t) = 6.353in 13.24ft

Span = 2.000 ft 50.00 ft

Weight = 34.00lbs 531250.00lbs

$\frac{WV}{\eta P}$ = 18.11

Aspect Ratio = 0.50

C_L = 0.085

C_{L_f} = 0.159

C_L = 0.958

α = 2.00

ϑ_f = 20.0

δ_f = 20.0

N_f = 2.0

$\frac{W}{S^{3/2}}$ = 1.503

$\frac{L_a}{L_f}$ = 25.0

Figure 6d - Computer-Generated Plots of the Test Results for the Highest - η_T Cases

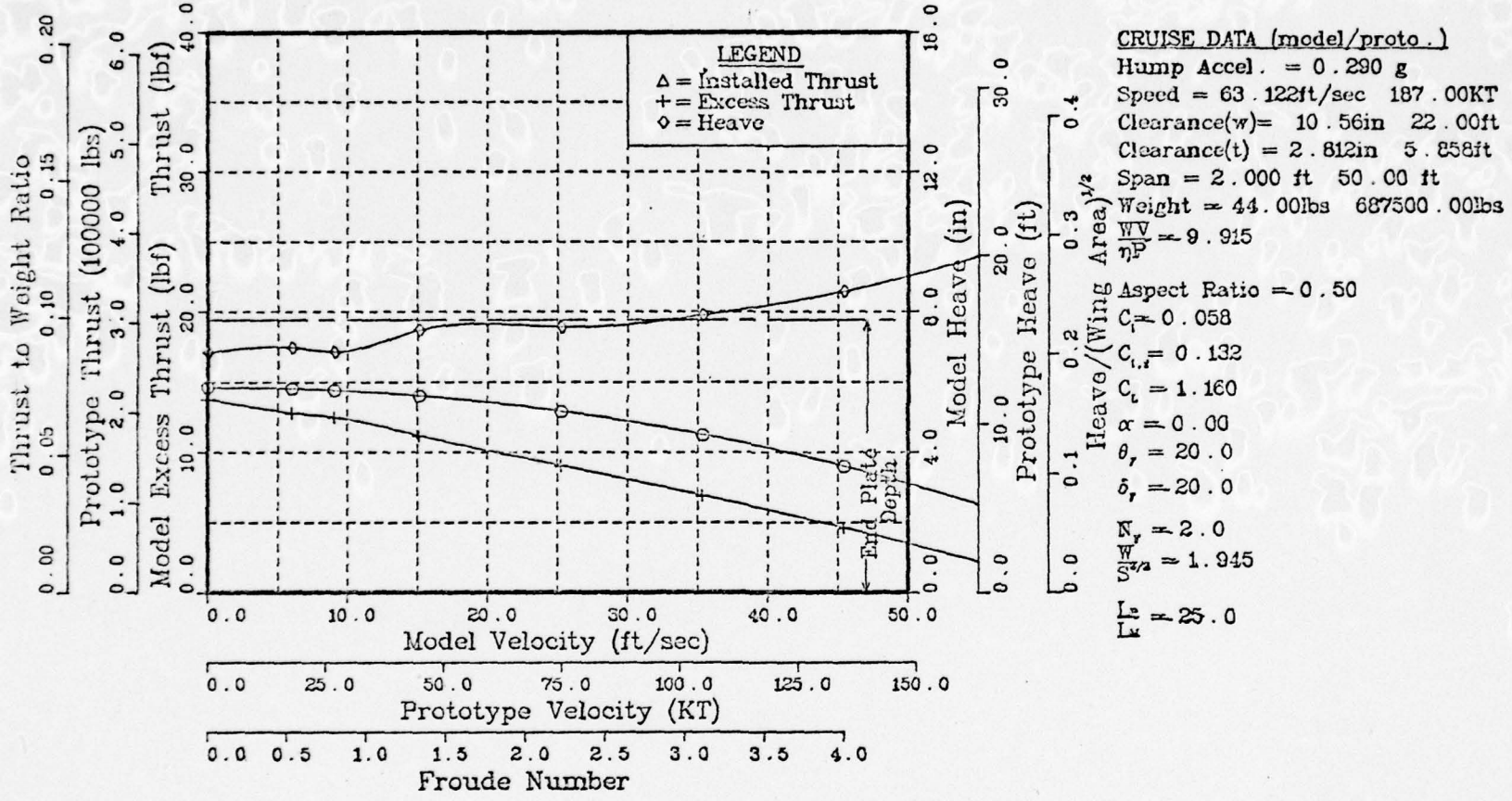
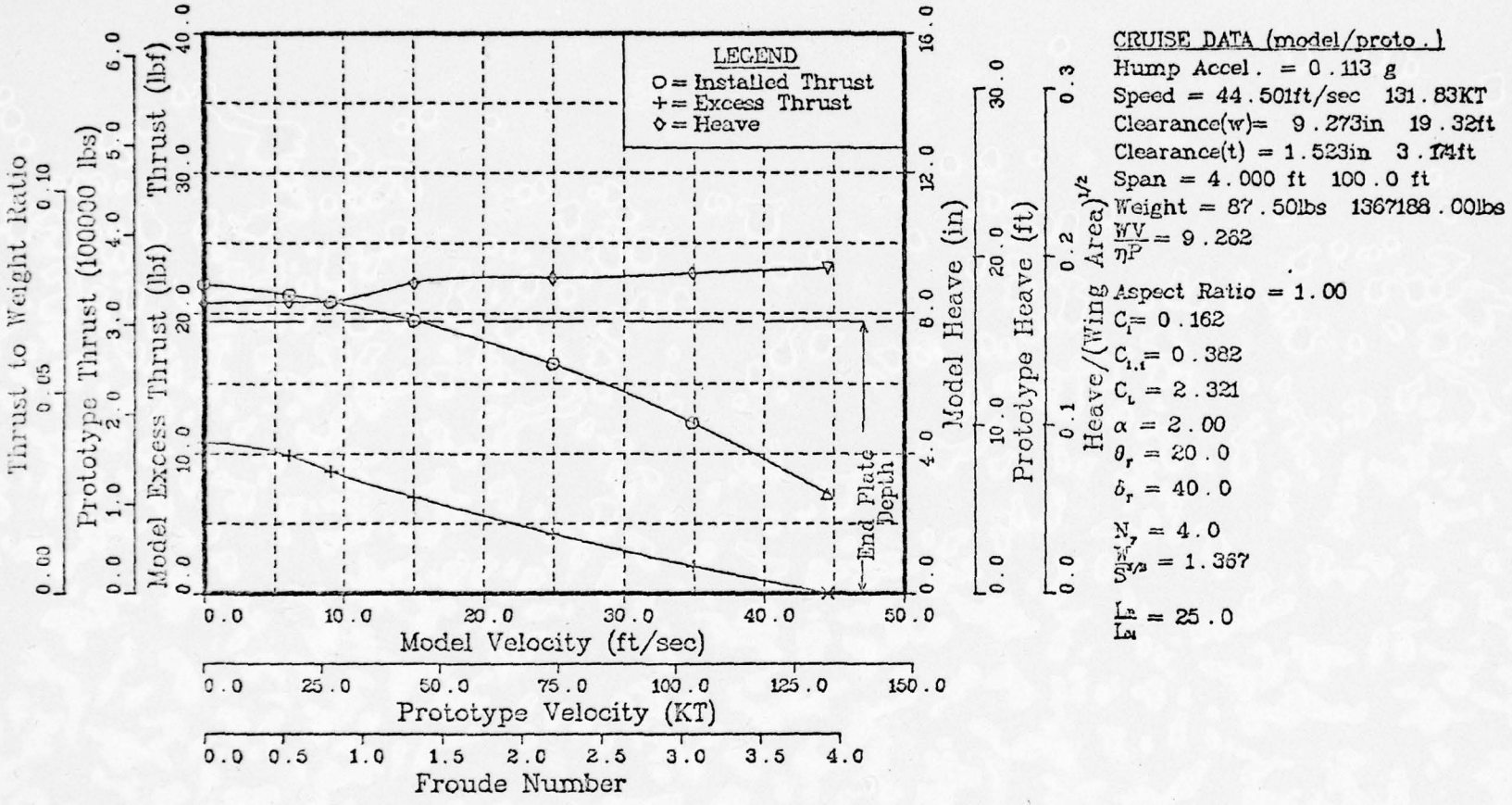


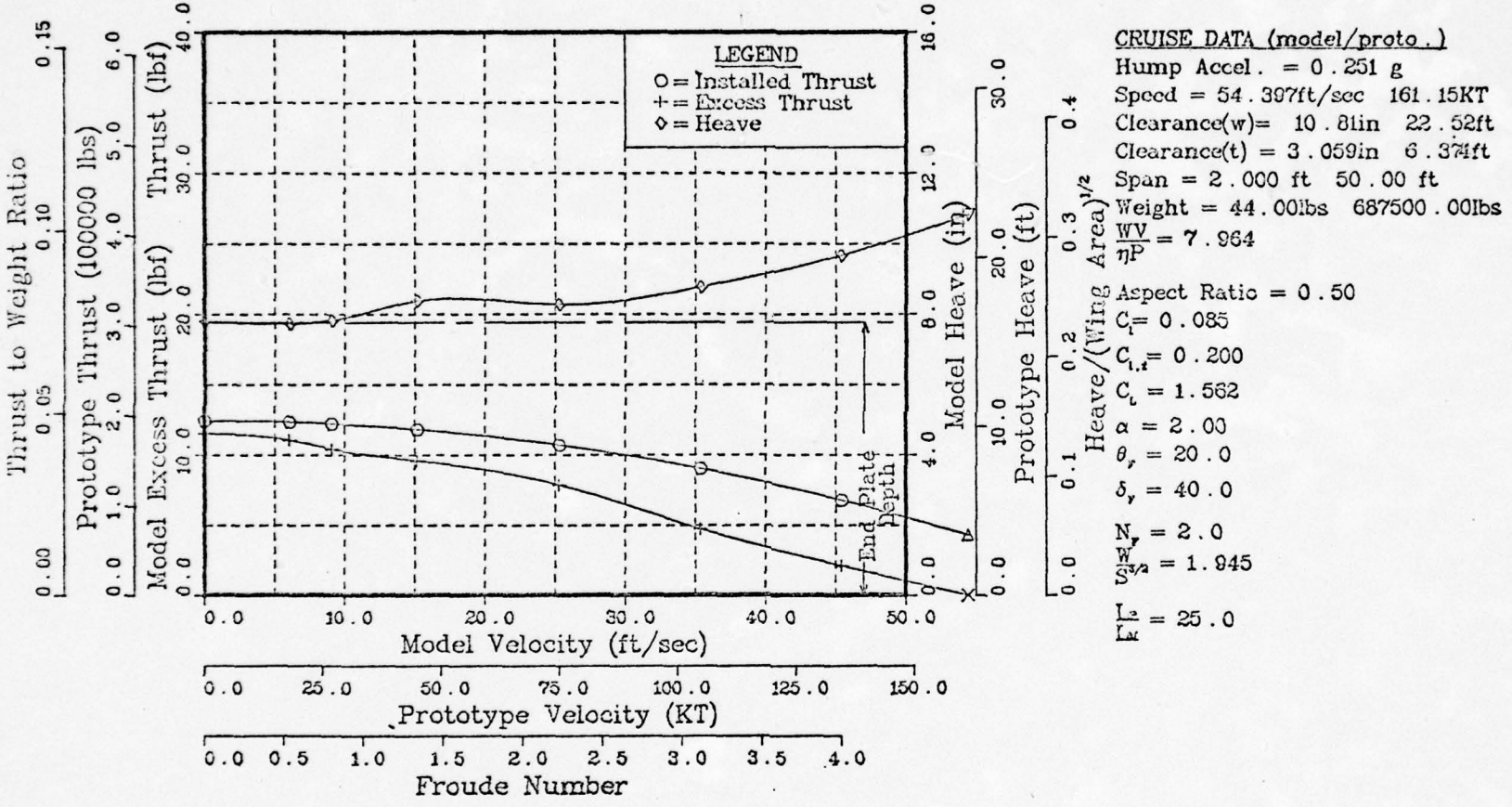
Figure 6e - Computer-Generated Plots of the Test Results for the Highest - η_T Cases



CRUISE DATA (model/proto.)
Hump Accel. = 0.113 g
Speed = 44.501ft/sec 131.83KT
Clearance(w)= 9.273in 19.32ft
Clearance(t) = 1.523in 3.174ft
Span = 4.000 ft 100.0 ft
Weight = 87.50lbs 1367188.00lbs
$\frac{WV}{\eta P}$ = 9.262

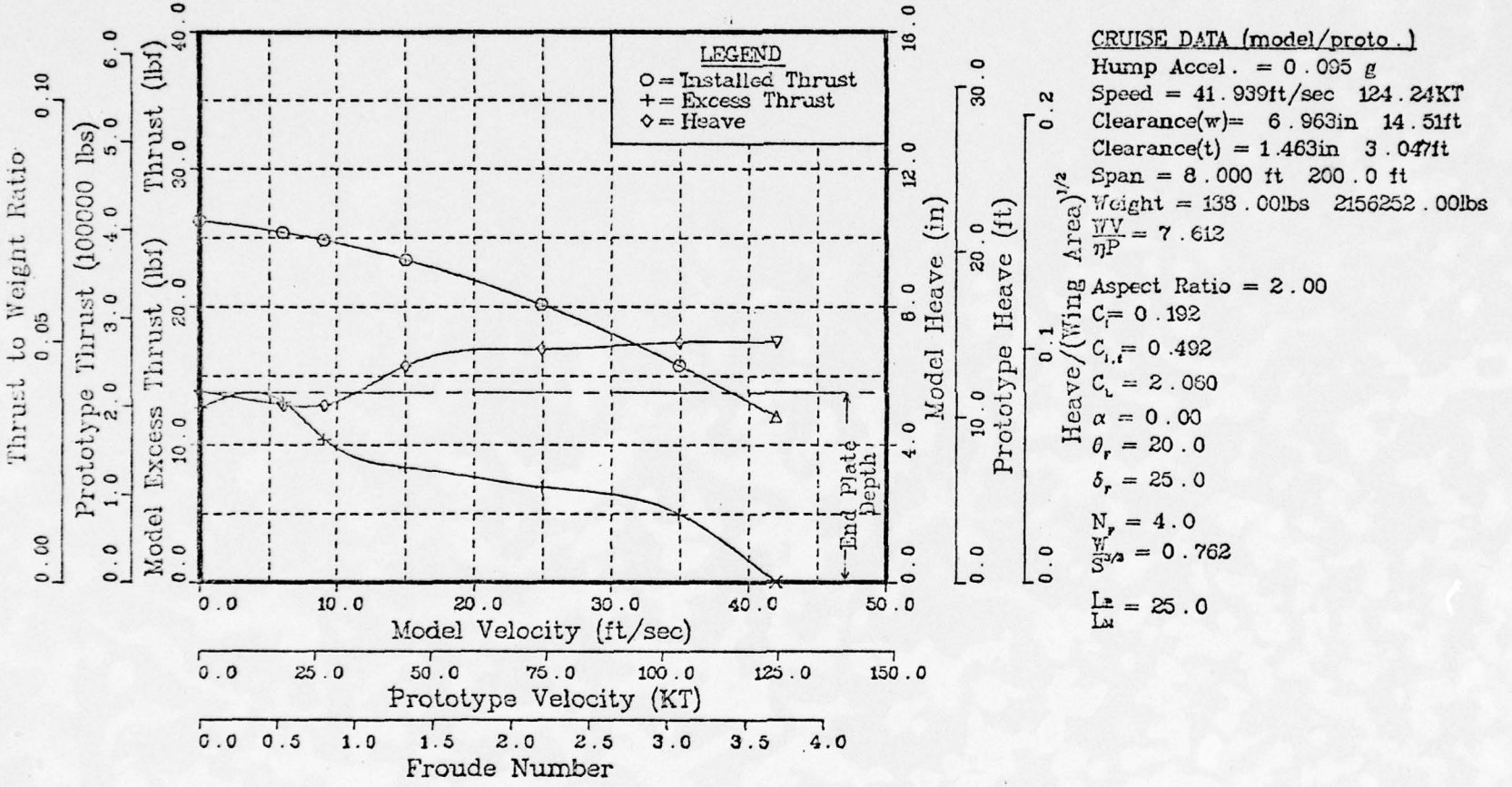
Aspect Ratio = 1.00
C_T = 0.162
C_{L_T} = 0.382
C_L = 2.321
α = 2.00
θ_r = 20.0
δ_r = 40.0
N_z = 4.0
$S_{\sqrt{S}}$ = 1.367
$\frac{L_E}{L_R}$ = 25.0

Figure 6f - Computer-Generated Plots of the Test Results for the Highest - η_T Cases



CRUISE DATA (model/proto.)
Hump Accel. = 0.251 g
Speed = 54.397ft/sec 161.15KT
Clearance(w)= 10.81in 22.52ft
Clearance(t) = 3.059in 6.374ft
Span = 2.000 ft 50.00 ft
Weight = 44.00lbs 687500.00lbs
$\frac{WV}{\eta P} = 7.964$
Aspect Ratio = 0.50
$C_L = 0.085$
$C_{L_f} = 0.200$
$C_t = 1.562$
$\alpha = 2.00$
$\theta_f = 20.0$
$\delta_f = 40.0$
$N_f = 2.0$
$\frac{W}{S^{3/2}} = 1.945$
$\frac{L_a}{L_M} = 25.0$

Figure 6g - Computer-Generated Plots of the Test Results for the Highest - η_T Cases



CRUISE DATA (model/proto.)

Hump Accel. = 0.095 g

Speed = 41.939ft/sec 124.24KT

Clearance(w)= 6.963in 14.51ft

Clearance(t) = 1.463in 3.047ft

Span = 8.000 ft 200.0 ft

Weight = 138.00lbs 2156252.00lbs

$\frac{WV}{\eta P}$ = 7.612

Aspect Ratio = 2.00

C_T = 0.192

C_{L_t} = 0.492

C_{L_r} = 2.060

α = 0.00

θ_r = 20.0

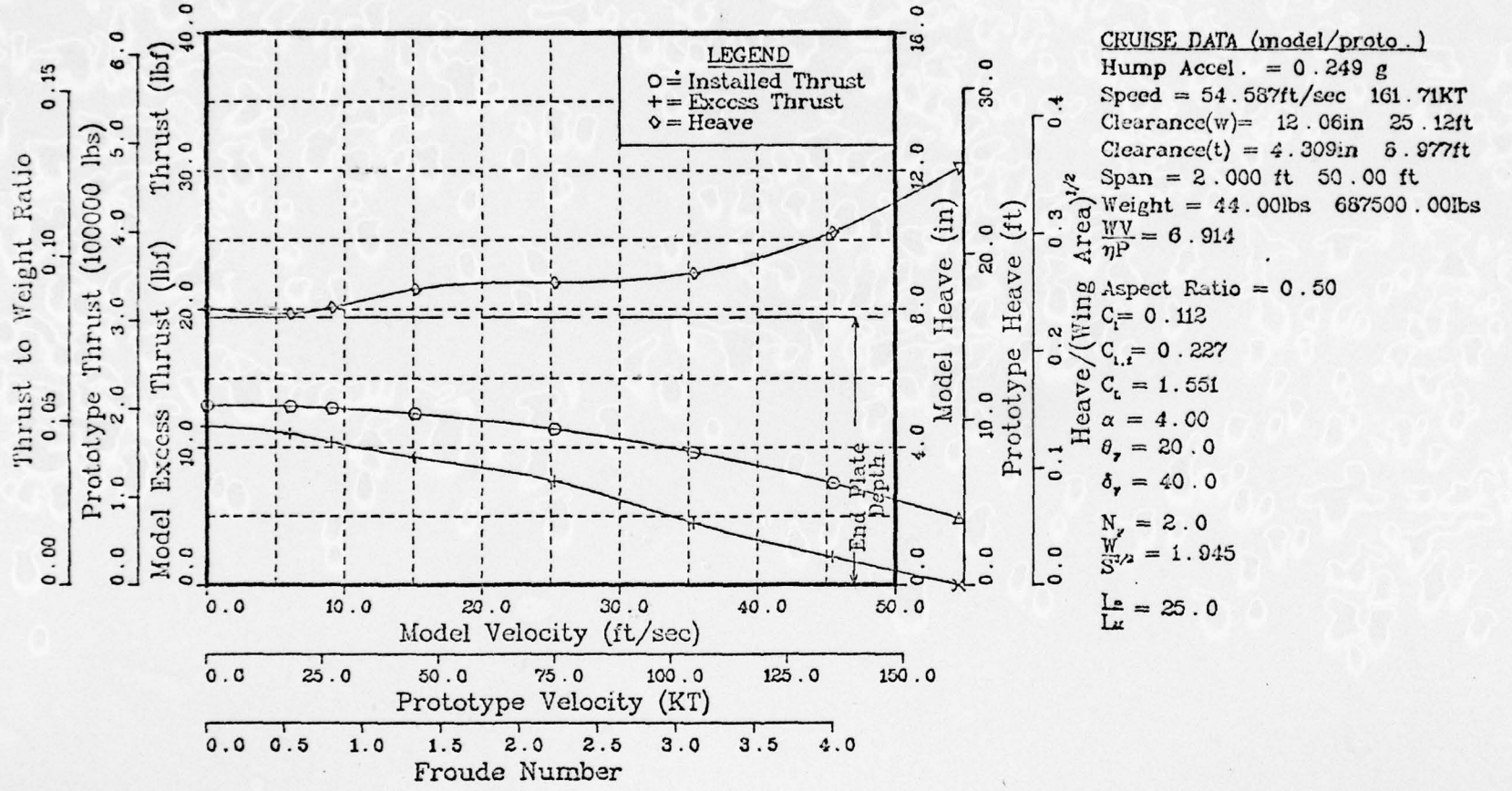
δ_r = 25.0

N_r = 4.0

$\frac{W}{S^{3/2}}$ = 0.762

$\frac{L_B}{L_M}$ = 25.0

Figure 6h - Computer-Generated Plots of the Test Results for the Highest - η_T Cases



CRUISE DATA (model/proto.)
Hump Accel. = 0.249 g
Speed = 54.587ft/sec 161.71KT
Clearance(w)= 12.06in 25.12ft
Clearance(t) = 4.309in 8.977ft
Span = 2.000 ft 50.00 ft
Weight = 44.00lbs 687500.00lbs
$\frac{WV}{\eta P} = 6.914$
Aspect Ratio = 0.50
$C_L = 0.112$
$C_{L_f} = 0.227$
$C_t = 1.551$
$\alpha = 4.00$
$\theta_f = 20.0$
$\delta_f = 40.0$
$N_z = 2.0$
$\frac{W}{S^{3/2}} = 1.945$
$\frac{L_e}{L_\alpha} = 25.0$

Figure 6i - Computer-Generated Plots of the Test Results for the Highest - η_T Cases

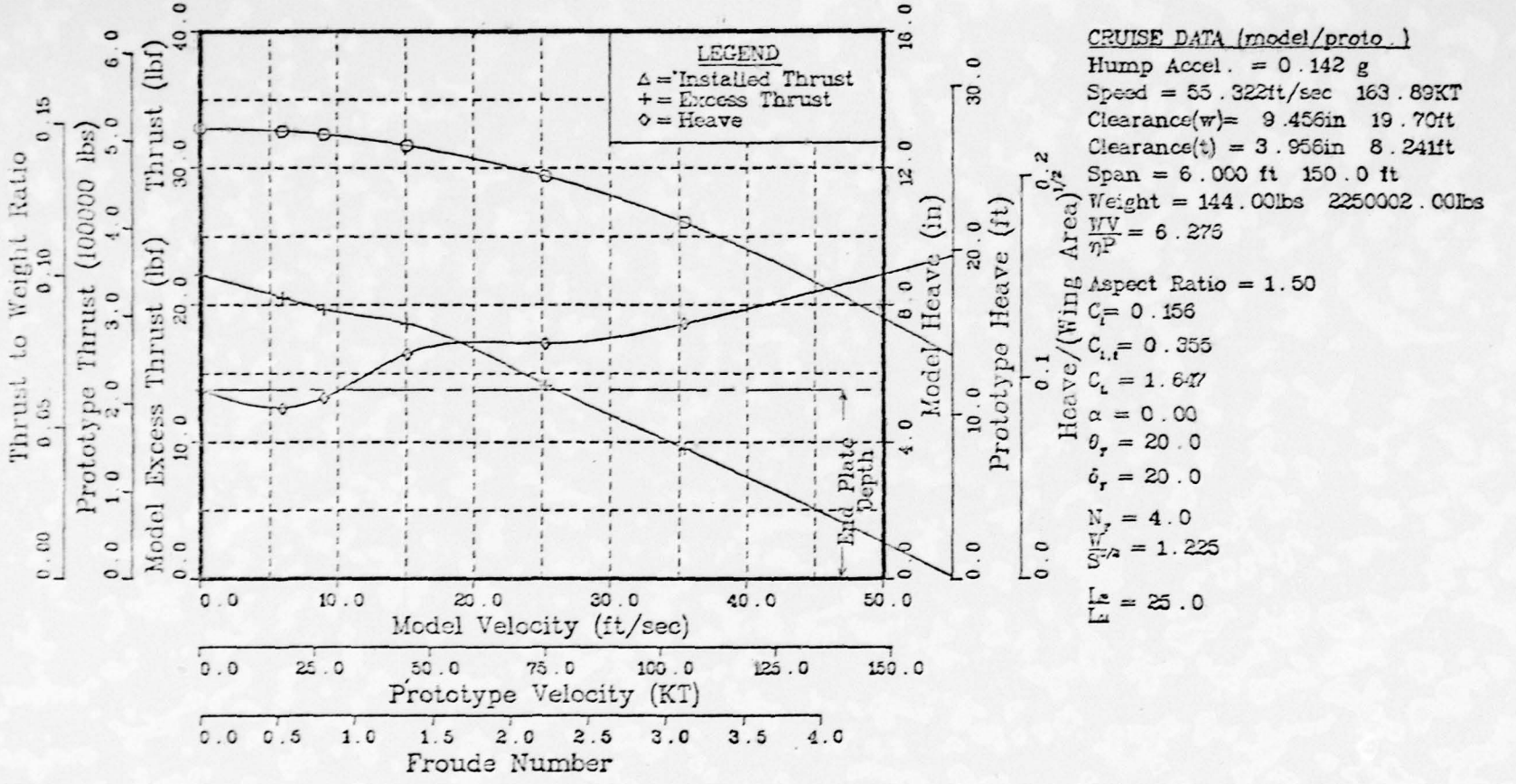


Figure 6j - Computer-Generated Plots of the Test Results for the Highest - η_T Cases

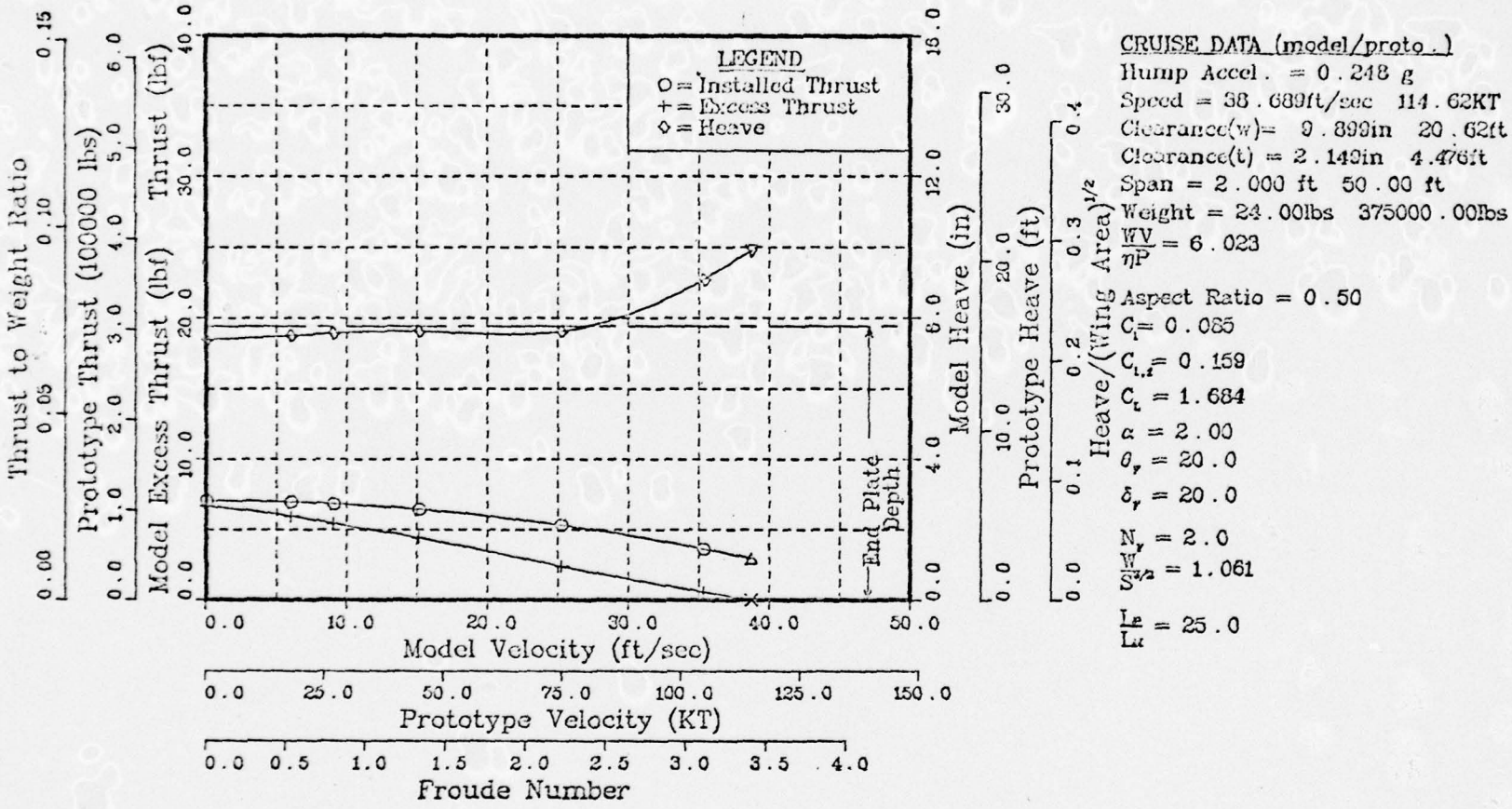


Figure 6k - Computer-Generated Plots of the Test Results for the Highest - η_T Cases

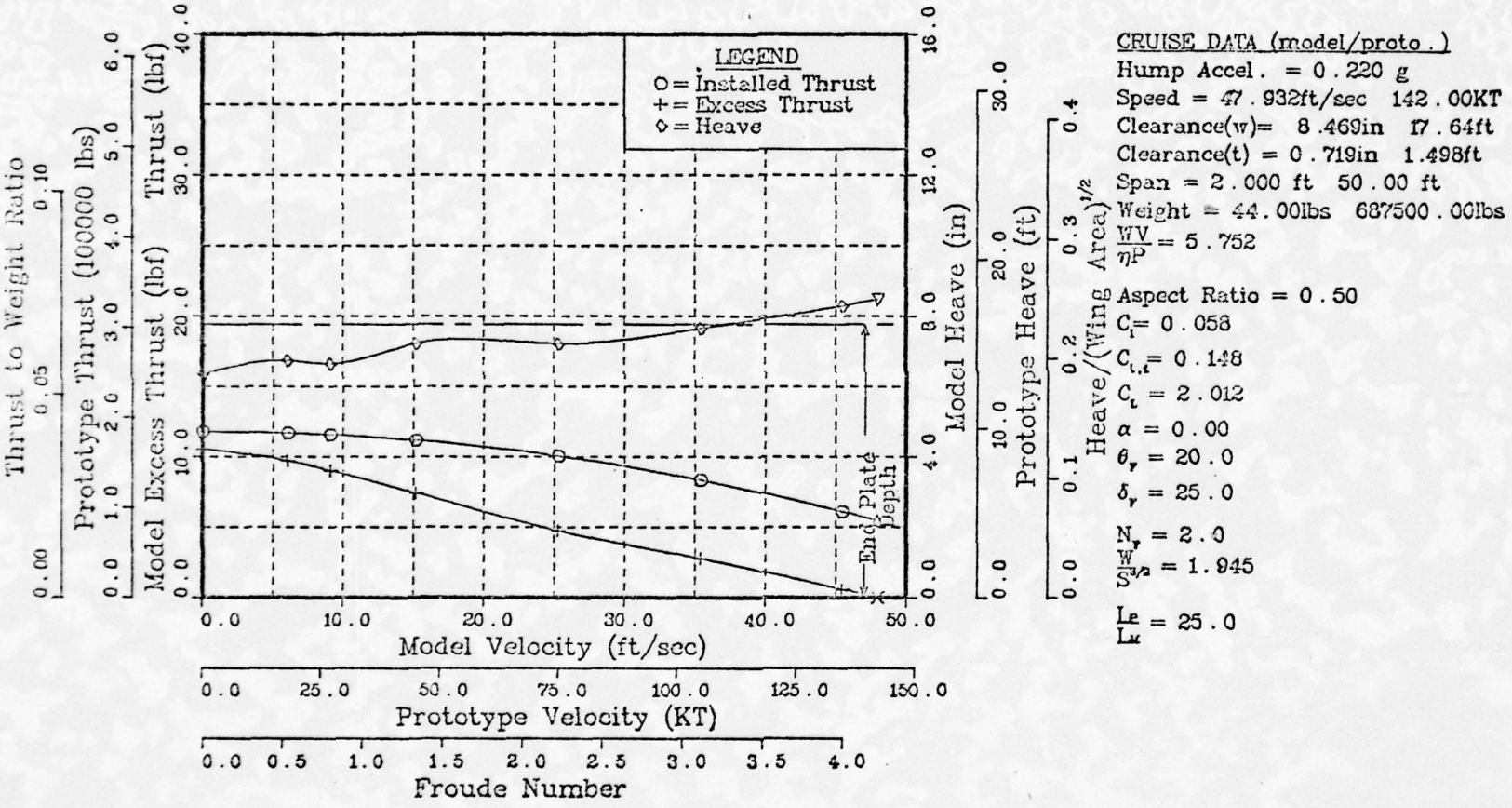


Figure 6ℓ - Computer-Generated Plots of the Test Results for the Highest - η_T Cases

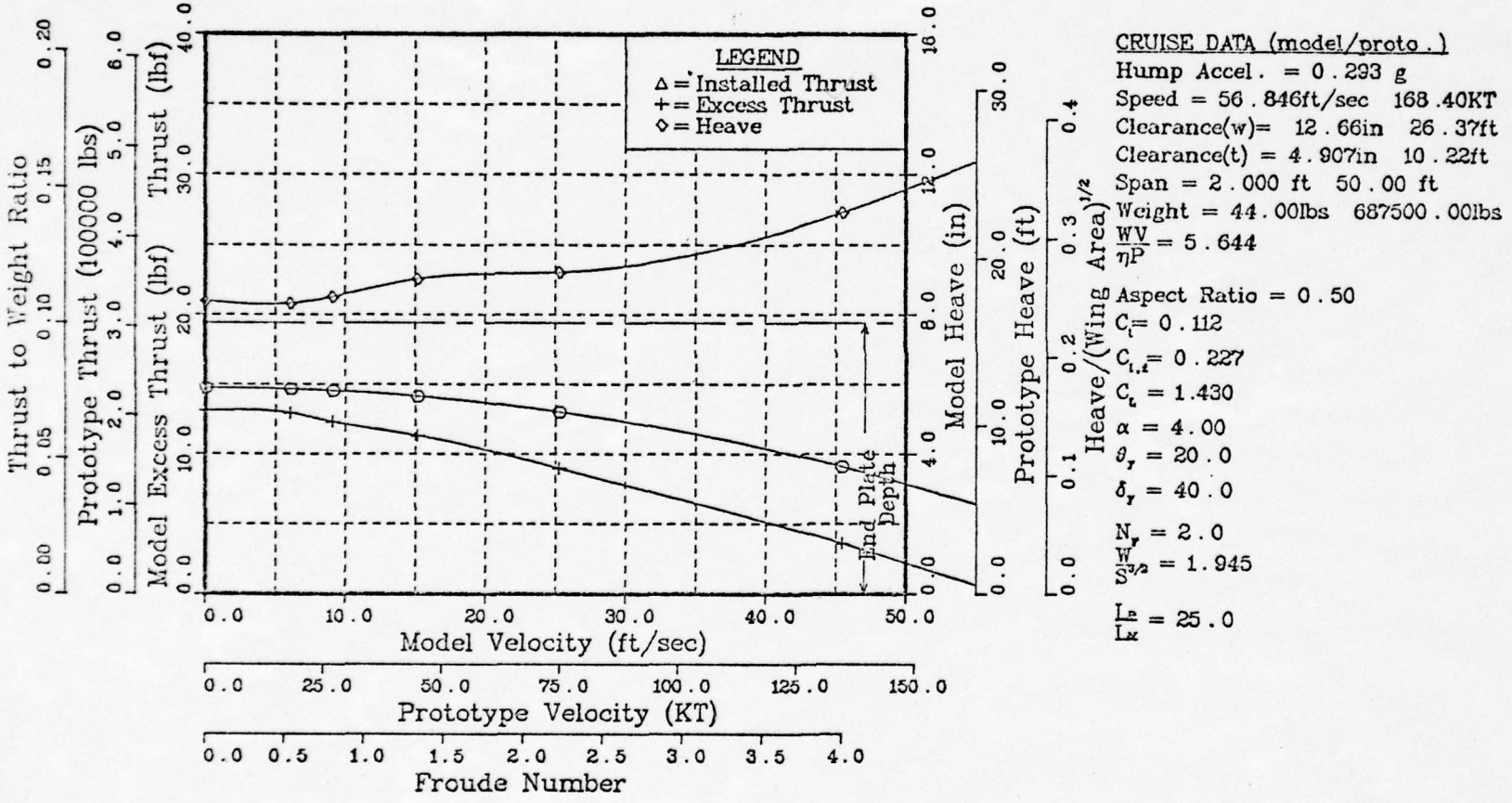


Figure 6m - Computer-Generated Plots of the Test Results for the Highest - η_T Cases

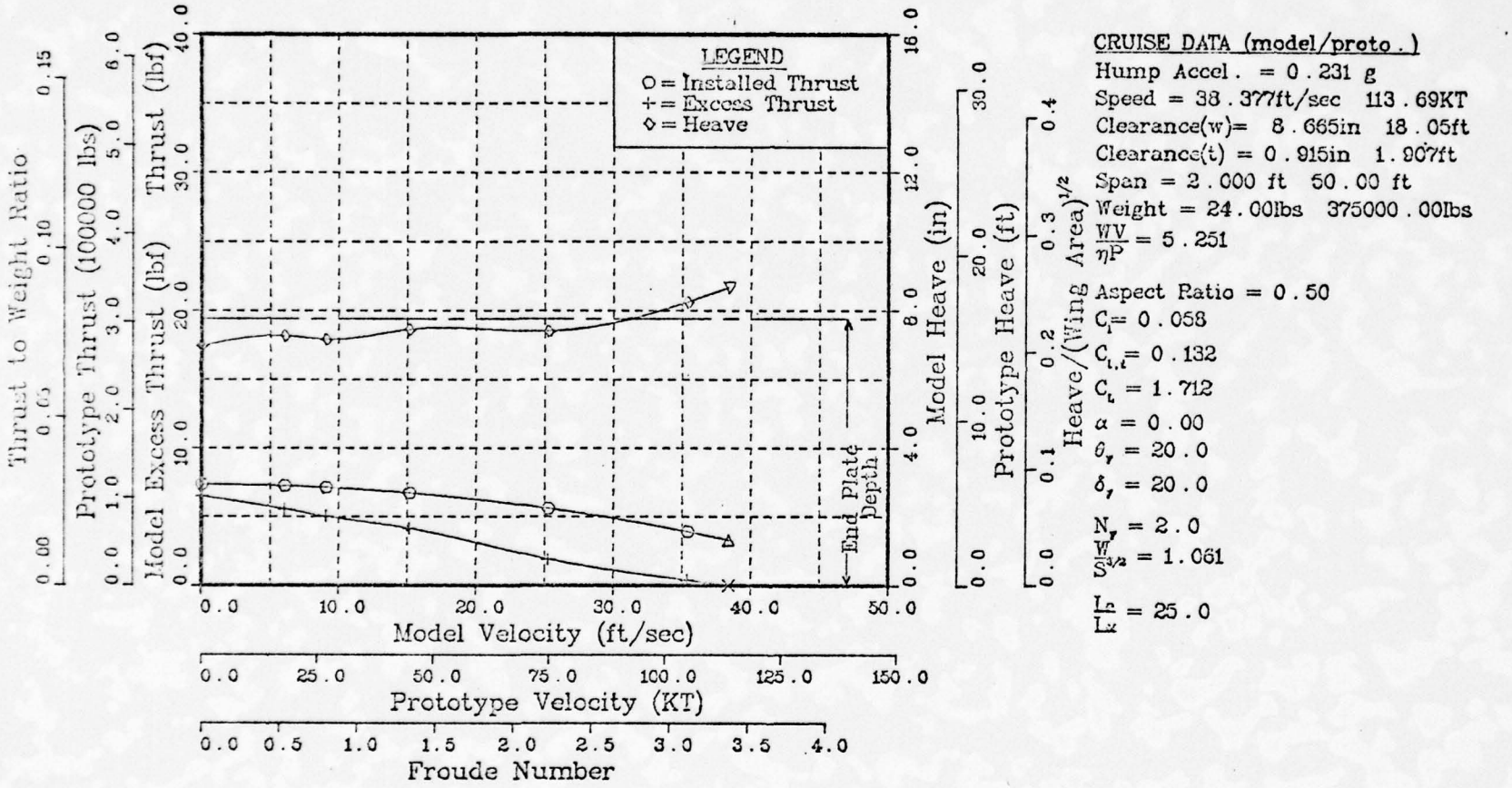
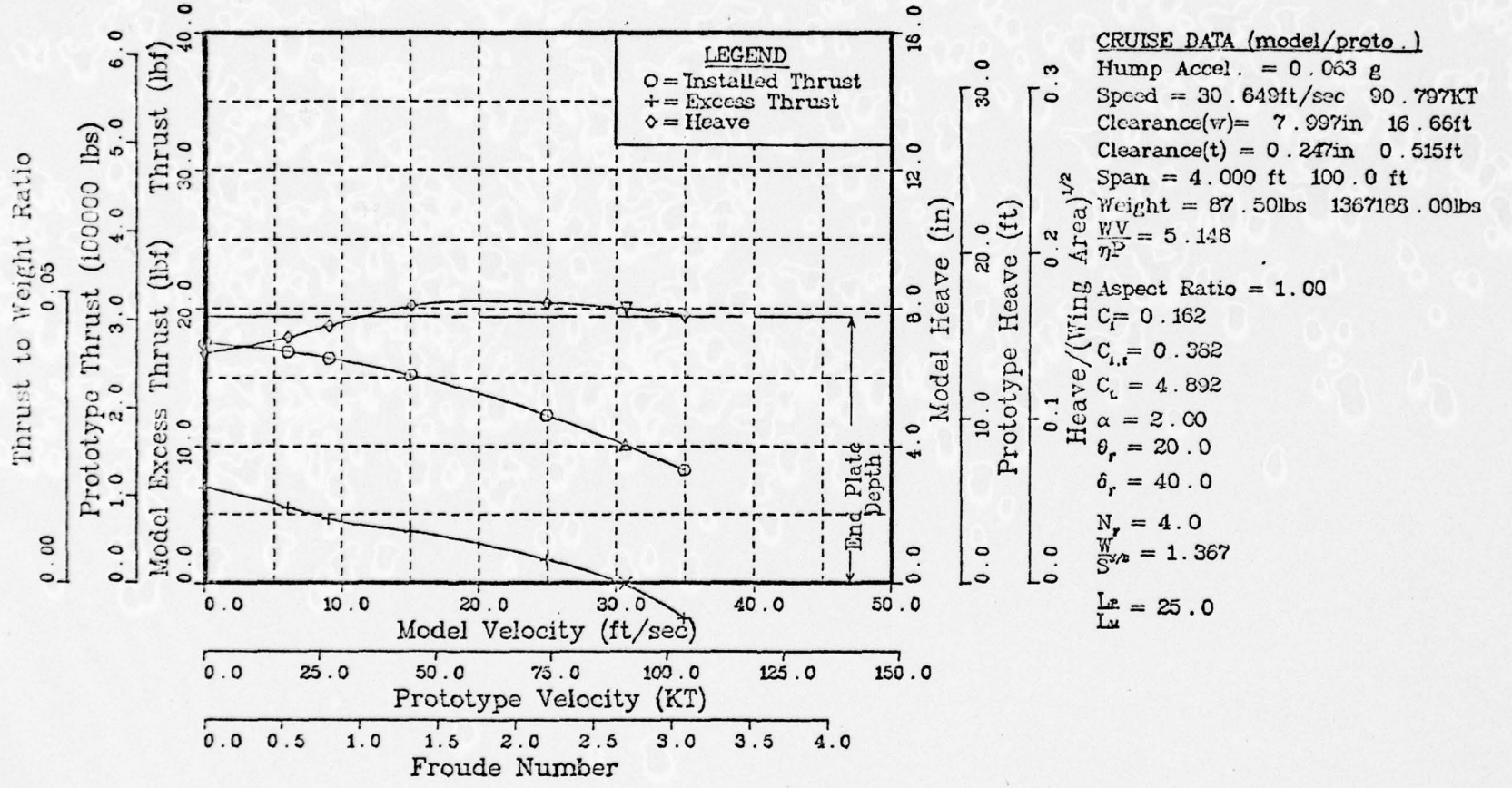


Figure 6n - Computer-Generated Plots of the Test Results for the Highest - η_T Cases



CRUISE DATA (model/proto.)

Hump Accel. = 0.063 g

Speed = 30.649ft/sec 90.797KT

Clearance(w)= 7.997in 16.66ft

Clearance(t) = 0.247in 0.515ft

Span = 4.000 ft 100.0 ft

Weight = 87.50lbs 1367188.00lbs

$\frac{WV}{\eta\upsilon}$ = 5.148

Aspect Ratio = 1.00

C_L = 0.162

$C_{L,t}$ = 0.362

C_r = 4.892

α = 2.00

θ_r = 20.0

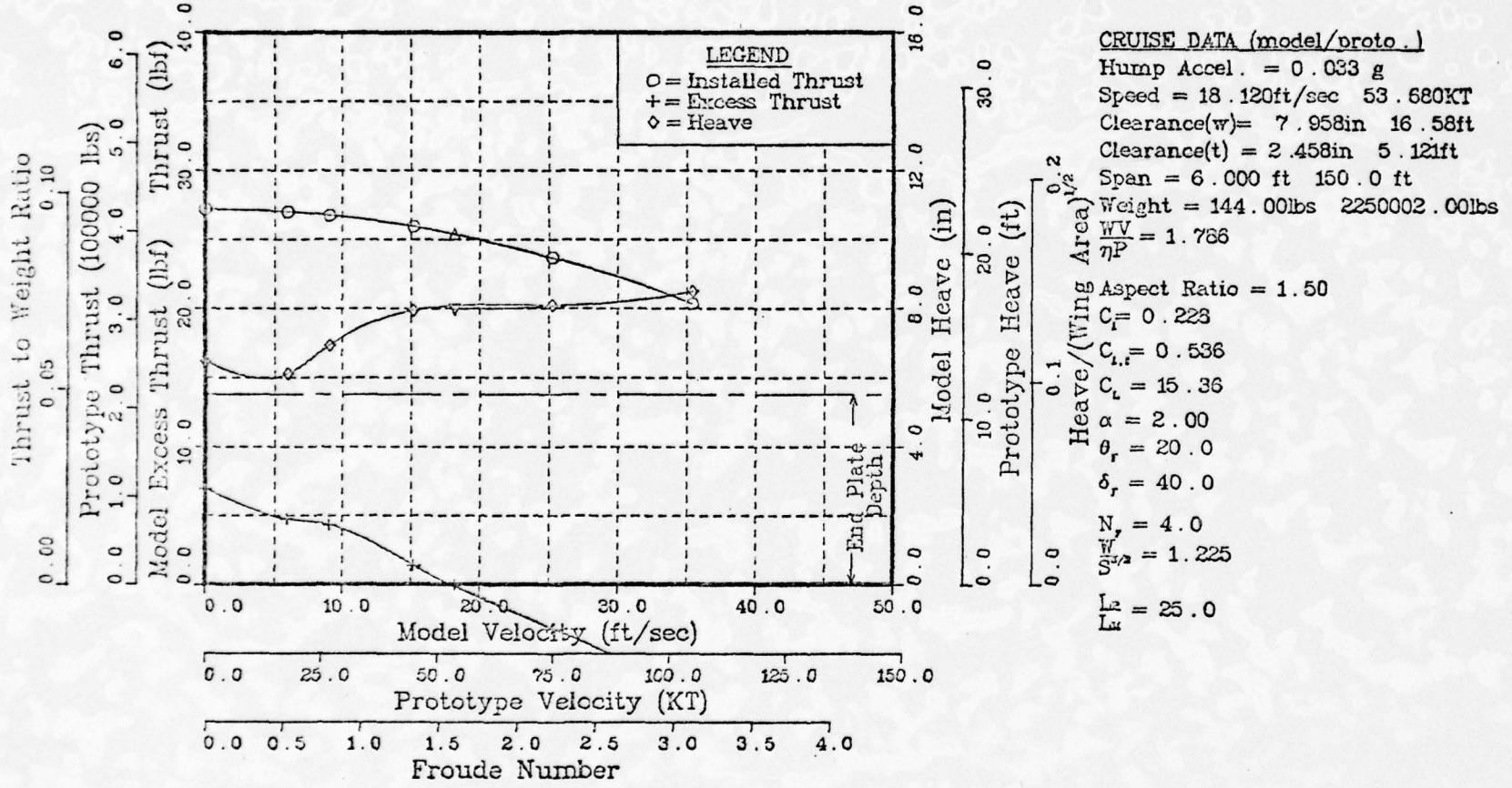
δ_r = 40.0

N_r = 4.0

$\frac{W}{S^{3/2}}$ = 1.367

$\frac{L_R}{L_M}$ = 25.0

Figure 6p - Computer-Generated Plots of the Test Results for the Highest - η_T Cases



CRUISE DATA (model/proto.)
Hump Accel. = 0.033 g
Speed = 18.120ft/sec 53.680KT
Clearance(w)= 7.958in 16.58ft
Clearance(t) = 2.458in 5.121ft
Span = 6.000 ft 150.0 ft
Weight = 144.00lbs 2250002.00lbs
$\frac{WV}{\eta P}$ = 1.786
Aspect Ratio = 1.50
C_r = 0.223
$C_{L,t}$ = 0.536
C_L = 15.36
α = 2.00
θ_r = 20.0
δ_r = 40.0
N_z = 4.0
$\frac{W}{S^{3/2}}$ = 1.225
$\frac{L_2}{L_1}$ = 25.0

Figure 6q - Computer-Generated Plots of the Test Results for the Highest - η_T Cases (low η_T case for comparison)

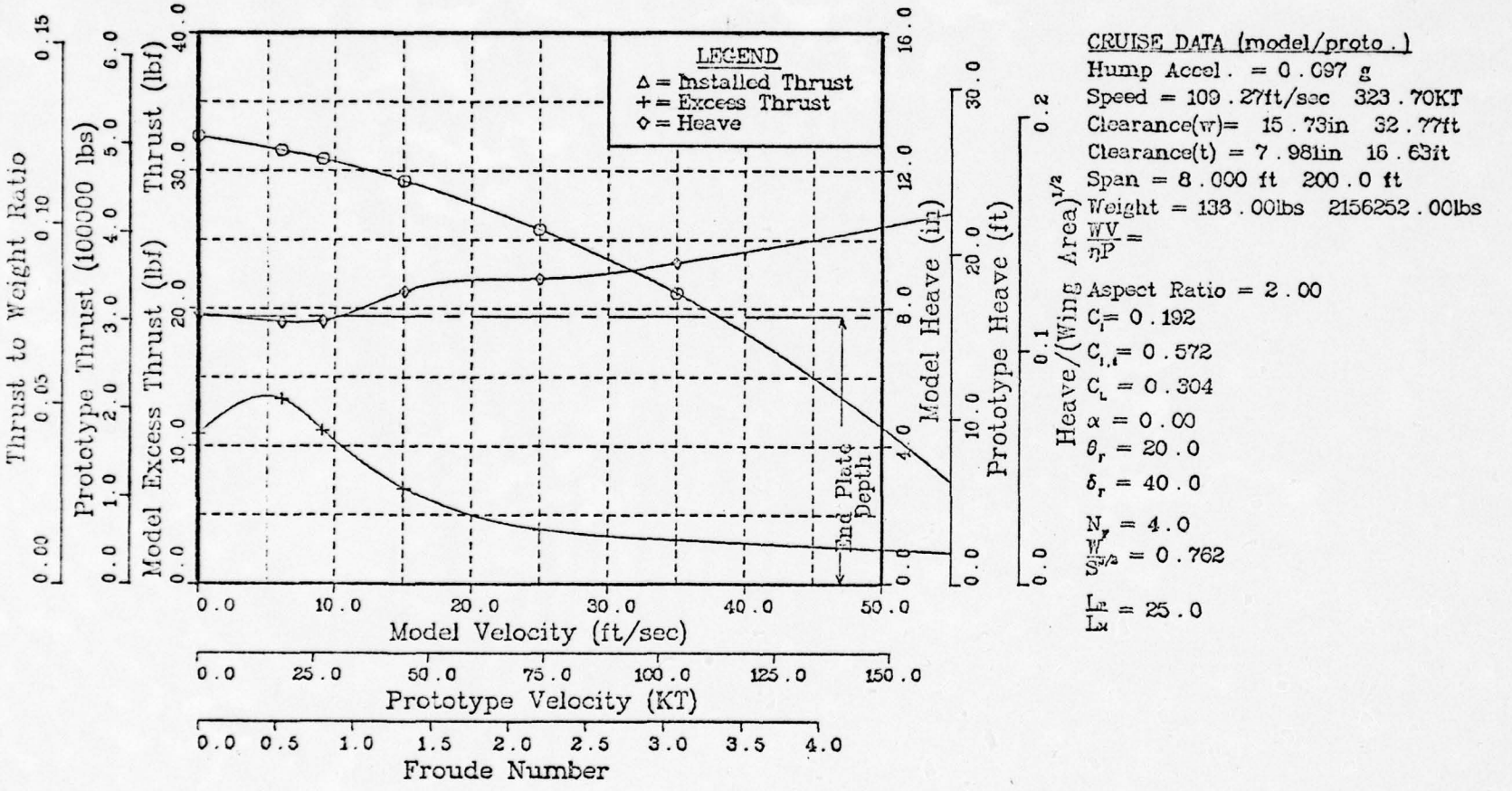
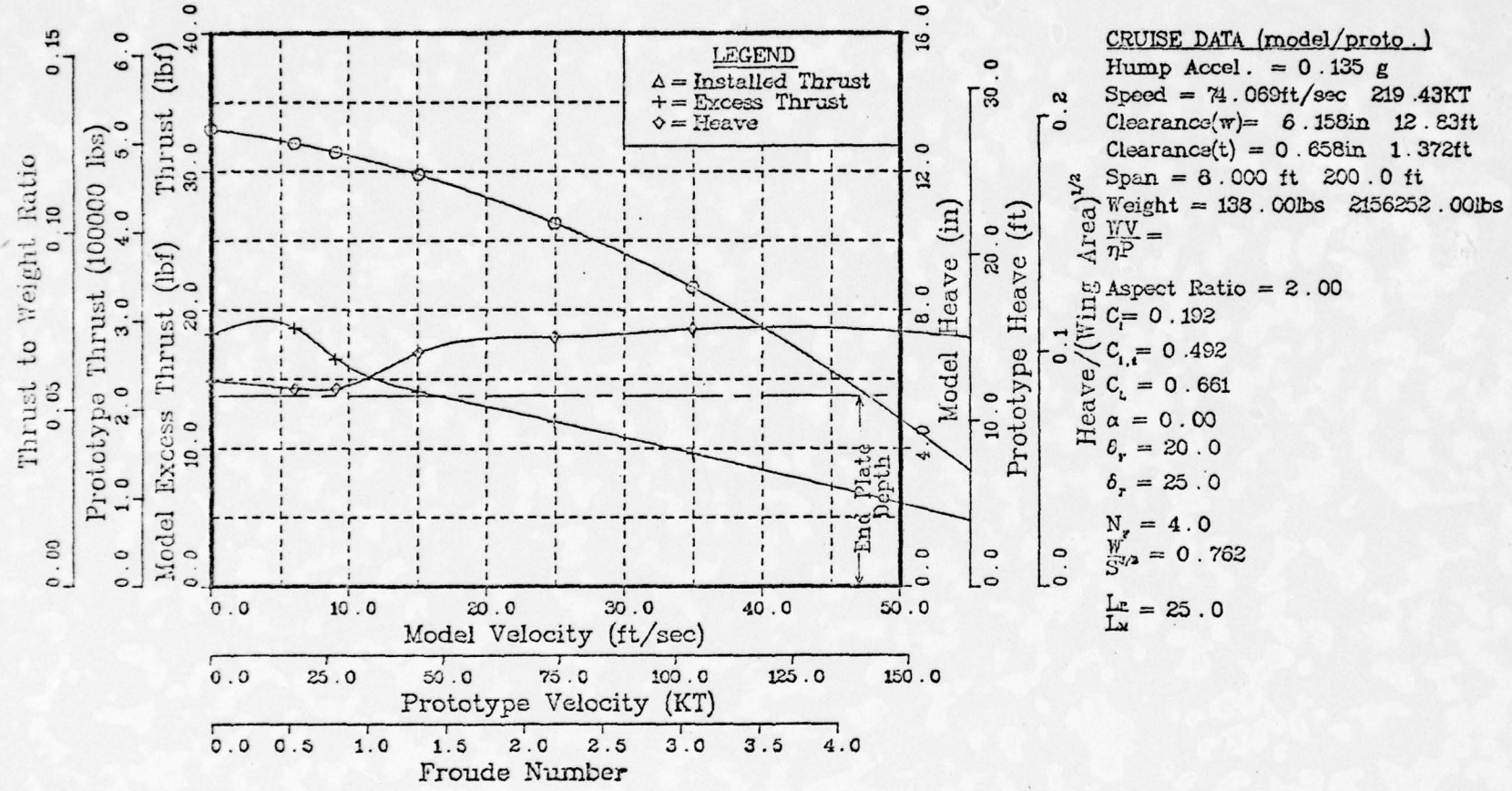


Figure 6r - Computer-Generated Plots of the Test Results for the Highest - η_T Cases (low η_T case for comparison)



CRUISE DATA (model/proto.)
Hump Accel. = 0.135 g
Speed = 74.069ft/sec 219.43KT
Clearance(w)= 6.158in 12.83ft
Clearance(t) = 0.658in 1.372ft
Span = 8.000 ft 200.0 ft
Weight = 138.00lbs 2156252.00lbs
$\frac{WV}{\eta P}$ =
Aspect Ratio = 2.00
C_T = 0.192
C_{L_t} = 0.492
C_L = 0.661
α = 0.00
δ_f = 20.0
δ_f = 25.0
N_p = 4.0
$\frac{W}{S^{1/2}}$ = 0.762
$\frac{L_E}{L_M}$ = 25.0

Figure 6s - Computer-Generated Plots of the Test Results for the Highest - η_T Cases (low η_T case for comparison)

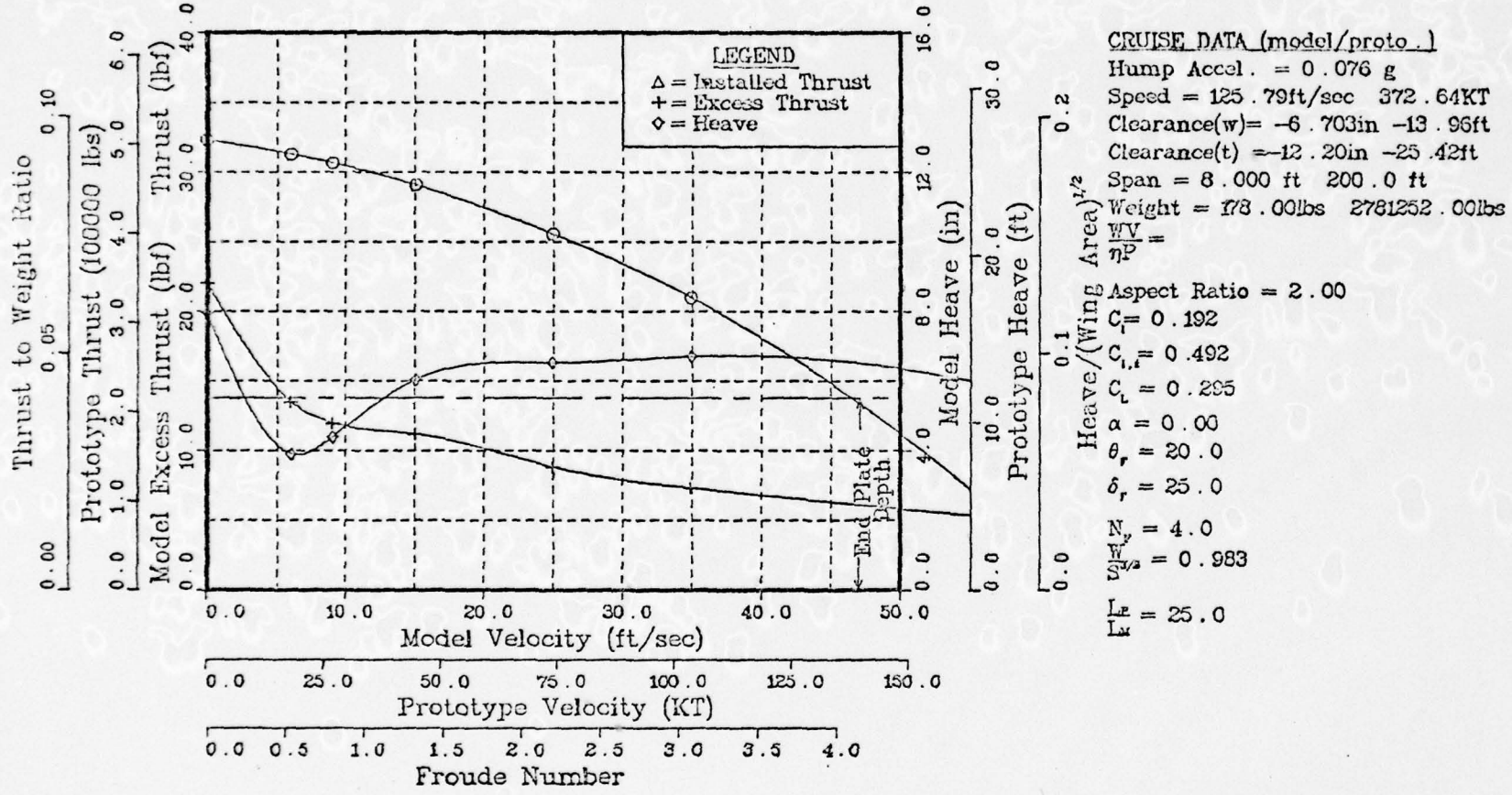


Figure 6t - Computer-Generated Plots of the Test Results for the Highest - η_T Cases (low η_T case for comparison)

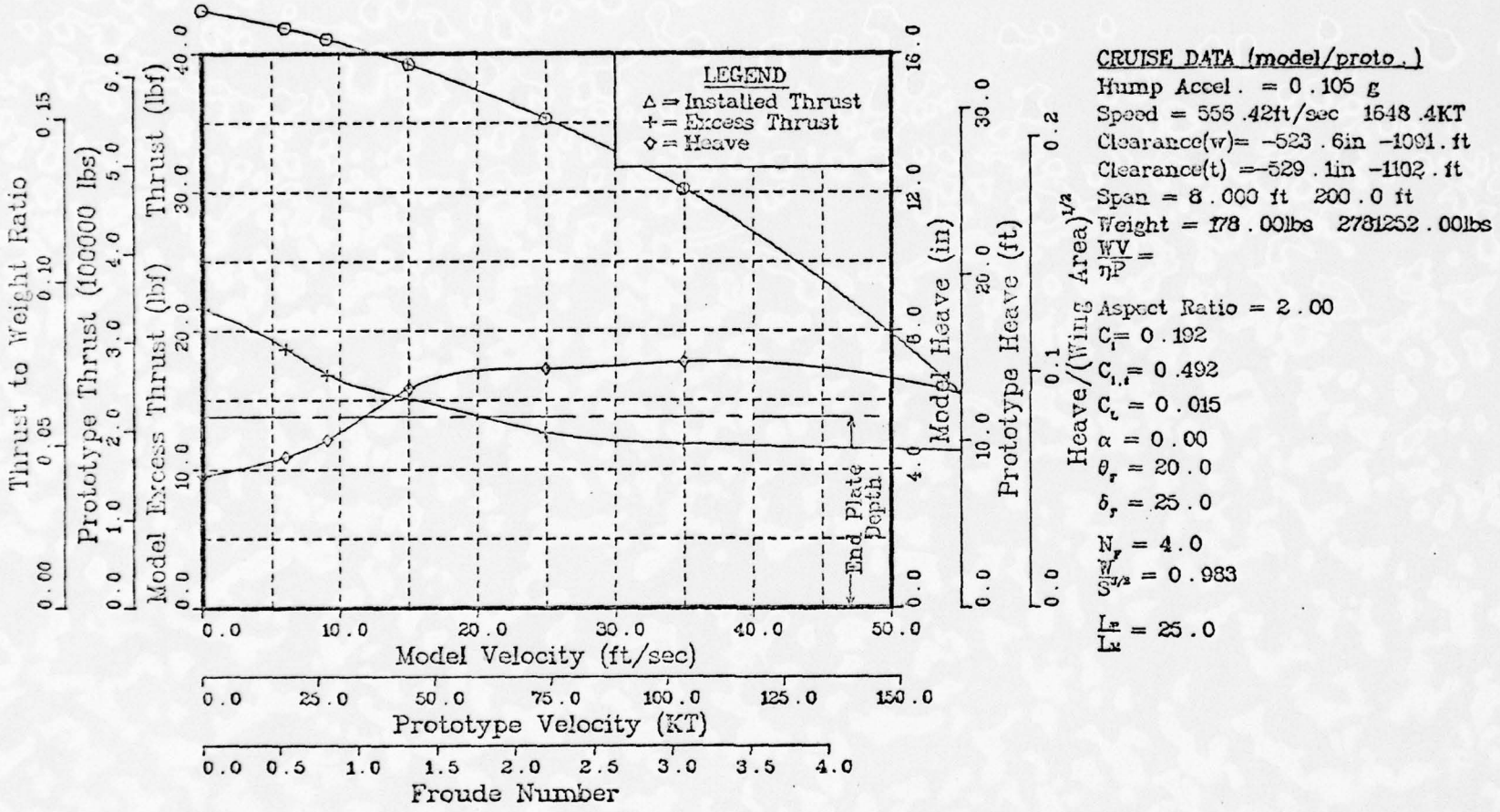


Figure 6u - Computer-Generated Plots of the Test Results for the Highest - η_T Cases (low η_T case for comparison)

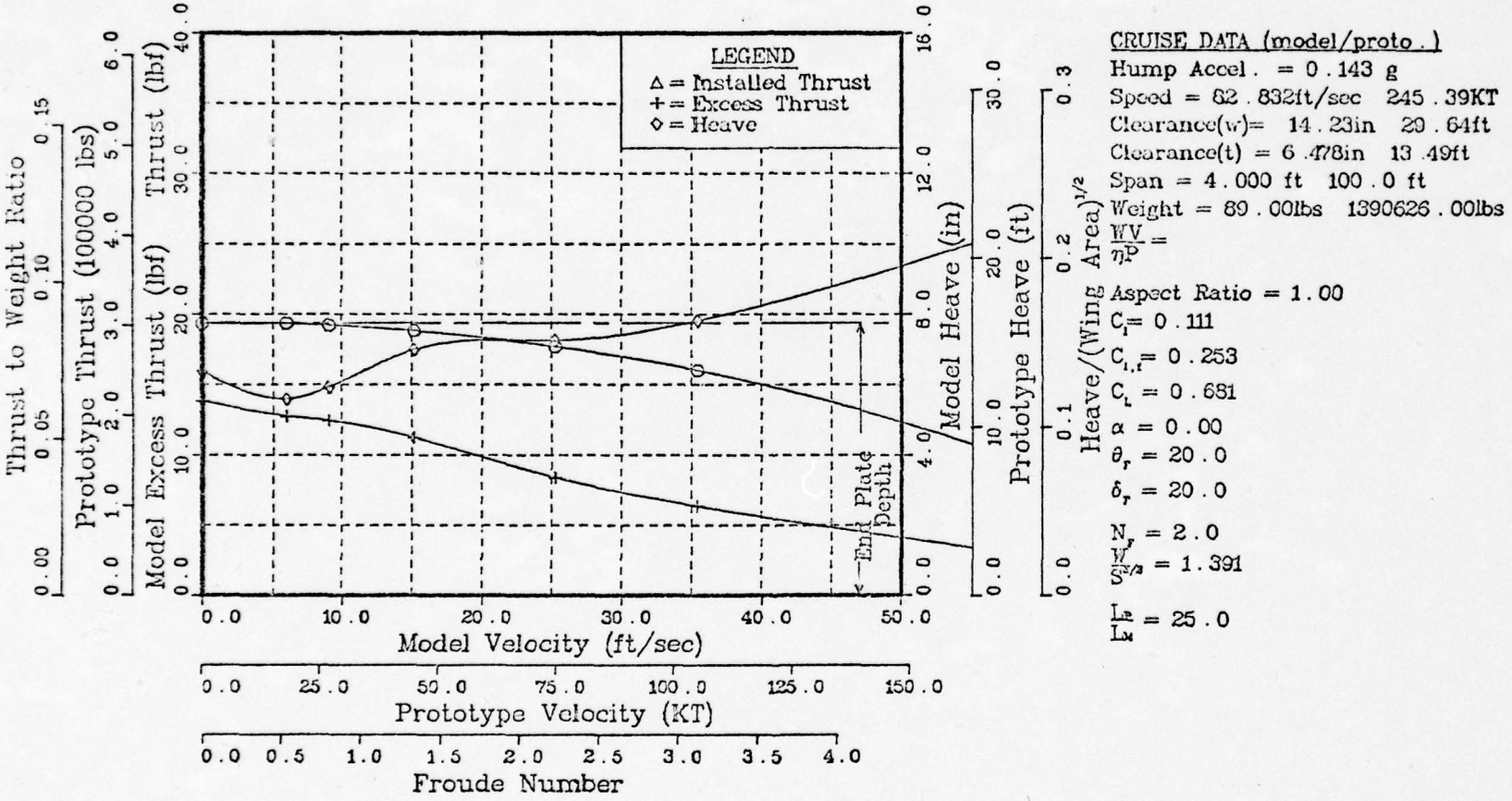


Figure 6v - Computer-Generated Plots of the Test Results for the Highest - η_T Cases (low η_T case for comparison)

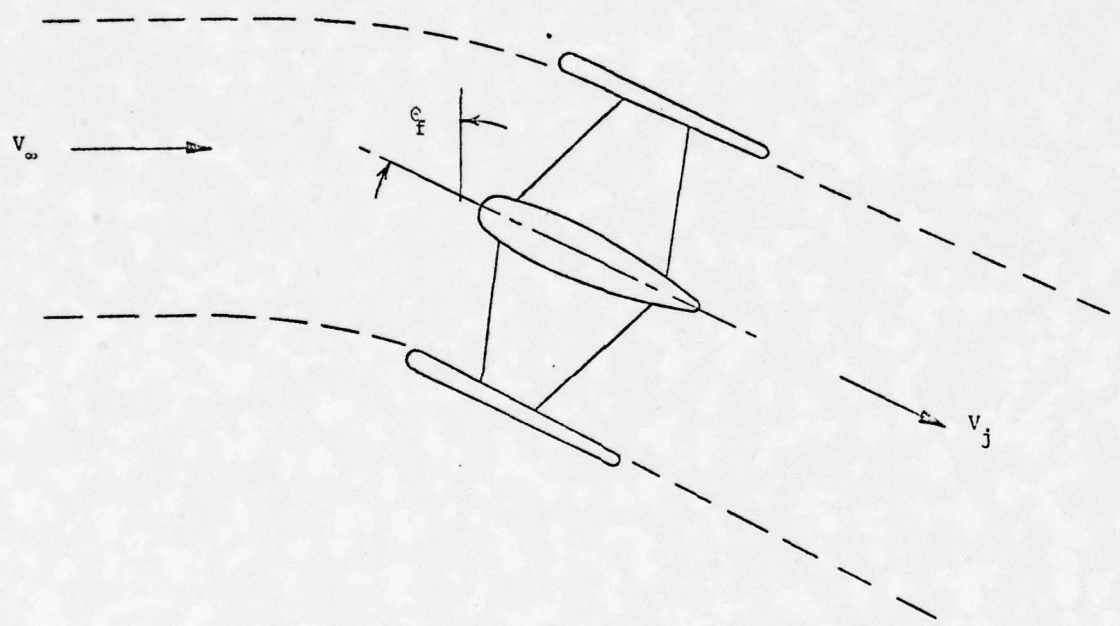


Figure 7 - Ducted-Fan Flow Model

TABLE 3 - LOSSES INCLUDED IN TRANSPORT EFFICIENCY

LOSS FEATURES INCLUDED

- o Froude inefficiency of propulsor
- o Propulsor inefficiency due to inclination
- o Friction, form, and induced drag on wing
- o Friction, form, and induced drag on fuselage
- o Induced drag on directed fans
- o Scrubbing drag on wing and fuselages
- o Separation drag over flap
- o Water wave drag
- o Wetting and spray drag

LOSS FEATURES NOT INCLUDED

- o Adiabatic inefficiency of ducted fan
- o Zero lift nacalle drag
- o Mechanical losses in transmission
- o Drag of aerodynamic or hydrodynamic stabilizers

TABLE 4 - TRANSPORT EFFICIENCY AND HEAVE DATA WITH RESPECT TO ASPECT RATIO

$\delta_f = 40^\circ$ W/S = 5.5 lb/ft^2 (26.8 kg/m^2)

$\theta_f = 20^\circ$ T/W = .210

$\alpha = 0^\circ$

A	h_{EP}, in. (cm)	$n_{f/b}$, fan/ft, (fan/m)	η_T	$h - h_{EP}$ in. (cm)
1/2	7.75 (19.68)	1 (.3)	3.19	-1.0 (-2.54)
3/4	5.50 (13.97)	2/3 (.2)	2.18	3.6 (9.14)
1	7.75 (19.68)	1 (.3)	2.08	-1.0 (-2.54)
1 1/2	5.50 (13.97)	2/3 (.2)	2.16	3.5 (8.89)
2	5.50 (13.97)	1/2 (.15)	3.49	2.8 (7.11)

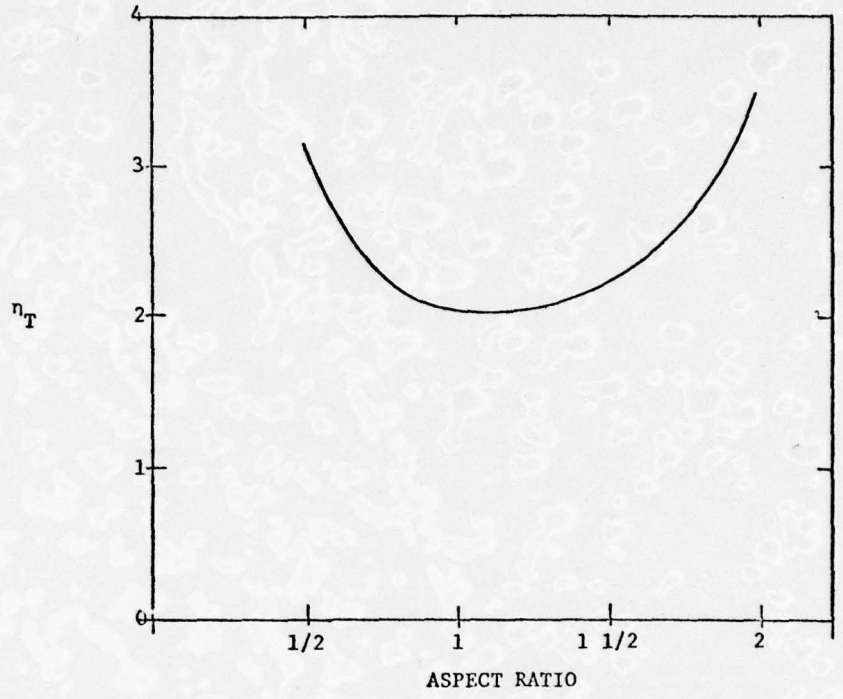


Figure 8a - Transport Efficiency vs. Aspect Ratio

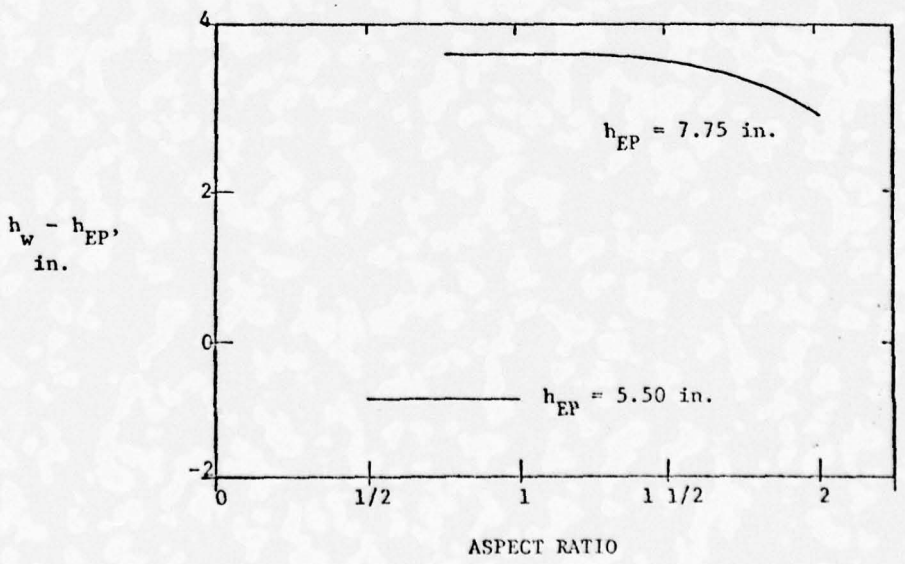


Figure 8b - End Plate Clearance vs. Aspect Ratio

TABLE 5 - TRANSPORT EFFICIENCY AND HEAVE DATA WITH RESPECT TO ANGLE OF ATTACK

$\epsilon_f = 20^o$ $\quad n_{f/b} = 1$ fan/ft (.3 fan/m)

W/S = 5.5 lb/ft^2 (26.8 kg/m^2) $\quad h_{EP} = 7.75$ in (19.68 cm)

A	α, deg	δ_f, deg	T/W	η_T	$h - h_{EP}$, in. (cm)
1/2	2	40	.283	7.96	3.06 (7.77)
	4		.297	6.91	4.31 (10.95)
1/2	0	20	.357	31.27	6.53 (16.59)
	2		.351	18.11	6.35 (16.13)
1	0	40	.255	29.16	1.43 (3.63)
	2		.252	9.26	2.15 (5.46)
1	0	40	.194	23.18	-0.20 (-0.51)
	2		.200	5.15	0.25 (0.63)

TABLE 6 - CONFIGURATIONS HAVING $\eta_T > 5.0$

η_T	A	α deg	δ_f deg	ϵ_f deg	W/S lb/ft^2 (kg/m^2)	T/W	$n_{f/b}$ fan/ft (fan/m)	h_{EP} in (cm)
31.27	1/2	0	20	20	4.3 (21.0)	.357	1 (.30)	7.75 (19.68)
29.16	1	0	40	20	5.5 (26.8)	.255	1	7.12 (18.08)
23.18	1	0	40	20	5.5 (26.8)	.194	1	7.75 (19.68)
18.11	1/2	2	20	20	4.3 (21.0)	.351	1	7.75
9.91	1/2	0	20	20	5.5 (26.8)	.333	1	7.75
9.26	1	2	40	20	5.5 (26.8)	.252	1	7.75
7.96	1/2	2	40	20	5.5 (26.8)	.283	1	7.75
7.61	2	0	25	20	4.3 (21.0)	.190	1/2 (.25)	5.50 (13.97)
6.91	1/2	4	40	20	5.5 (26.8)	.297	1	7.75 (19.68)
6.02	1/2	2	20	20	3.0 (14.6)	.294	1	7.75
5.75	1/2	0	25	20	5.5 (26.8)	.268	1	7.75
5.64	1/2	4	40	20	5.5 (26.8)	.335	1	7.75
5.35	1 1/2	0	40	20	6.0 (29.3)	.228	1	7.75
5.25	1/2	0	20	20	3.0 (14.6)	.306	1	7.75
5.15	1	2	40	20	5.5 (26.8)	.200	1	7.75

TABLE 7 - HEAVE DATA WITH RESPECT TO FLAP DEFLECTION ANGLE

$A = 1/2$ $\quad n_{f/b} = 1$ fan/ft (.3 fan/m)

$\theta_f = 20^o$ $\quad h_{EP} = 7.75$ in (19.68) CM)

δ_f deg	α deg	W/S lb/ft^2(kg/m^2)	T/W	$h_w - h_{EP}$ in (cm)	V_{TRIM} ft/sec (m/sec)
20	0	4.3 (21.0)	.35	6.53 (16.58)	62.5 (19.05)
40				2.46 (6.25)	42.3 (12.89)
20	.2	4.3 (21.0)	.35	6.35 (16.13)	61.1 (18.62)
40				2.51 (6.37)	40.2 (12.25)
20	0	3.0 (14.6)	.29	1.85 (4.70)	38.1 (11.61)
40				2.91 (7.39)	36.3 (11.06)
20	2	3.0 (14.6)	.29	2.14 (5.44)	38.7 (11.79)
40				1.37 (3.48)	30.6 (9.33)

TABLE 8 - TRANSPORT EFFICIENCY AND HEAVE DATA WITH RESPECT TO FAN ANGLE

$A = 1$	$W/S = 5.5$ lb/ft^2 (26.8 kg/m^2)
$\delta_f = 40^o$	$T/W = .24$
$\alpha = 0^o$	$n_{f/b} = 1$ fan/ft (.3 fan/m)

$h_{EP} = 7.75$ in (19.68 cm)

Θ_f deg	η_T	$h - h_{EP}$, in (cm)
15	6.26	- 0.25 (-0.63)
25	6.25	1.25 (3.17)
30	5.83	1.05 (2.67)
35	5.57	1.15 (2.92)
40	5.77	0.45 (1.14)

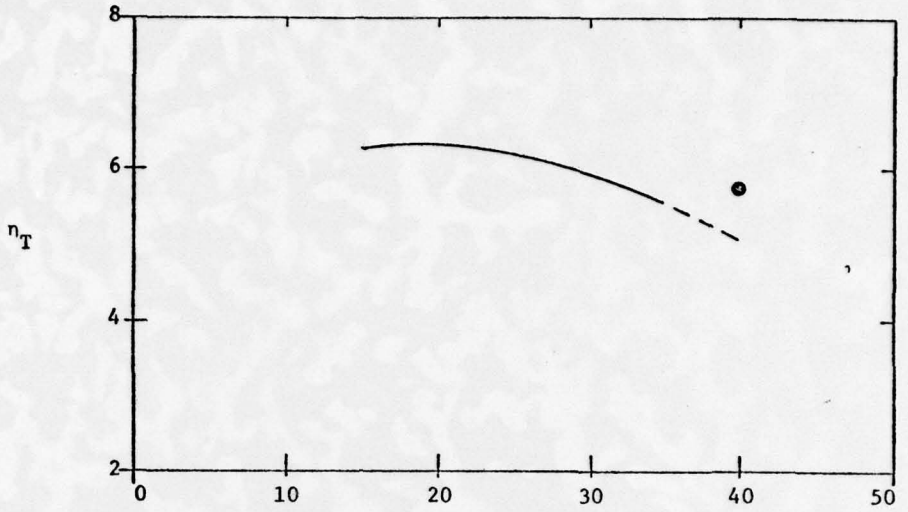


Figure 9a - Transport Efficiency vs. Fan Angle

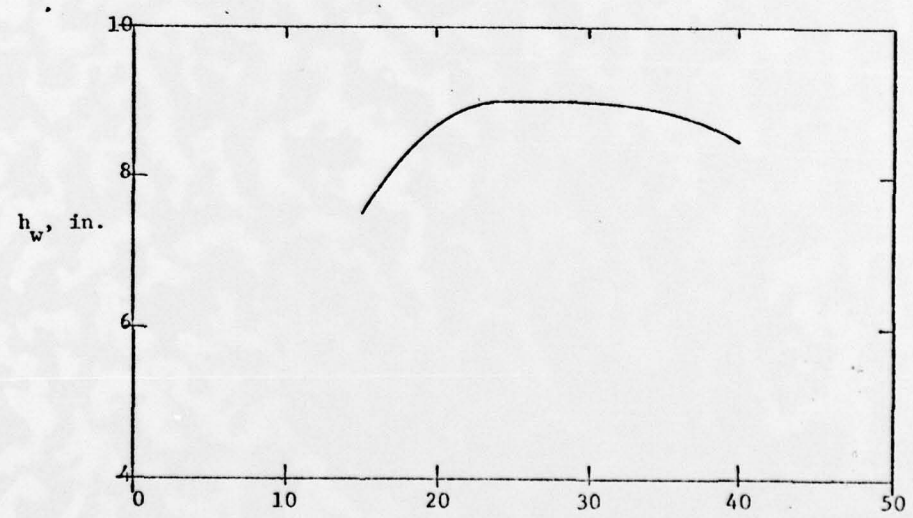


Figure 9b - Heave vs. Fan Angle

TABLE 9 - DIFFERENCES IN TRANSPORT EFFICIENCY DUE TO INCREASING WING LOADING FOR VARIOUS ASPECT RATIOS

A	W/S[1] RANGE FROM	TO	$\Delta \eta_T$ RANGE, %
1/2	3.0 (14.6)	5.5 (26.8)	70 - 139
3/4	4.3 (21.0)	6.0 (29.3)	-18 - 0
1	4.3 (21.0)	5.5 (26.8)	0 - 22
2	4.3 (21.0)	5.5 (26.8)	-4 - 20

[1] lb/ft^2 (kg/m^2)

TABLE 10 - DIFFERENCES IN TRANSPORT EFFICIENCY DUE TO INCREASE IN THRUST - WEIGHT RATIO

A	δ_f deg	Θ_f deg	α deg	W/S[1]	% Δ T/W	% Δ η_T	LOWER T/W η_T
1/2	20	20	0	4.3 (21.0)	.24	.72	5.75
1	40	20	2	5.5 (26.8)	.26	.80	9.26
1/2	40	20	4	5.5 (26.8)	.13	-.18	6.91
1/2	20	20	2	3.0 (14.6)	.30	-.31	6.02

[1] lb/ft^2 (kg/m^2)

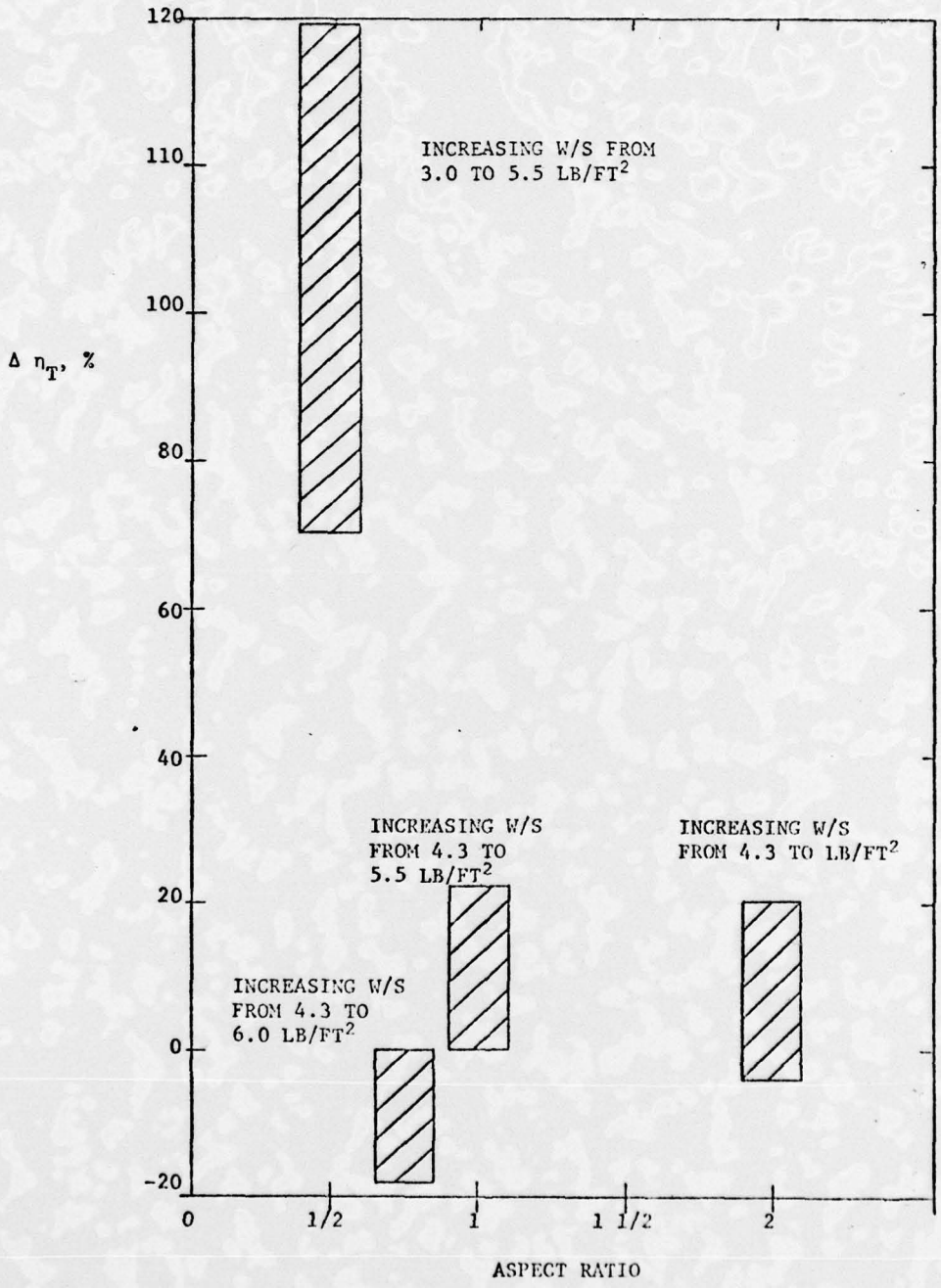


Figure 10 - Percentage Change in Transport Efficiency Due to Increasing W/S, for Several Aspect Ratios

TABLE 11 - TRANSPORT EFFICIENCY AND HEAVE DATA WITH RESPECT TO FAN DENSITY

$A = 1$	$T/W = .34$
$\Theta_f = 20^o$	$W/S = 5.5$ lb/ft^2 (26.8 kg/m^2)
$\delta_f = 40^o$	$h_{EP} = 7.75$ in (19.7 cm)

α deg	$n_{f/b} = 1/2$		$n_{f/b} = 1$	
	η_T	$h_w - h_{EP}$[1]	η_T	$h_w - h_{FP}$
0	1.66	2.79 (7.09)	2.29	2.98 (7.57)
0[2]	2.51	1.18 (3.0)	3.22	1.00 (2.54)
2	1.61	6.10 (15.50)	1.84	-0.77 (-1.96)
2[3]	2.30	2.58 (6.55)	2.95	1.32 (3.35)

[1] in (cm)

[2] $T/W = .22$

[3] $\delta_f = 20^o$

TABLE 12 - COMPARISON OF EXTREME-PERFORMANCE CONFIGURATIONS

	BEST PERFORMANCE η_T = 31.27, h_w = 14.28 in (.36m)	WORST PERFORMANCE η_T = 1.36, h_w = 7.96 (.20 m)
A	1/2	1 1/2
α	0^o	2^o [3]
δ_f	20^o [1]	40^o [3]
ζ_f	20^o [2]	20^o [2]
T/W	.357 [3]	.189
W/S	4.3 lb/ft^2 (21.0 kg/m^2)	6.0 lb/ft^2 (29.3 kg/m^2)
$n_{f/b}$	1 fan/ft (.30 fan/m)	2/3 fan/ft (.20 fan/m)

[1] Lowest value tested

[2] Essentially only value tested

[3] Highest value tested

TABLE 13 - TRANSPORT EFFICIENCY AND HEAVE DATA FOR SEVERAL ENDPLATE CONFIGURATIONS IN 2 SEA STATES

ENDPLATE DESIGN	T/W	η_T CALM	η_T SS5	$h_w - h_{EP}$, in (cm) CALM	$h_w - h_{EP}$, in (cm) SS5
METAL (RIGID)	.215	7.15	6.46	0.25 (.63)	0.70 (1.78)
BASIC (RIGID)	.250	29.16*	5.17	1.43 (3.63)	1.83 (4.65)
FLEXIBLE	.255	6.14	7.05	1.38 (3.50)	1.60 (4.06)

$A = 1$ $\quad \alpha = 0^o$

$\delta_f = 40^o$ $\quad W/S = 5.5$ lb/ft^2 (26.8 kg/m^2)

$\epsilon_f = 20^o$

* This singular point is either from perfect component matching or bad data and is not considered characteristic of the results

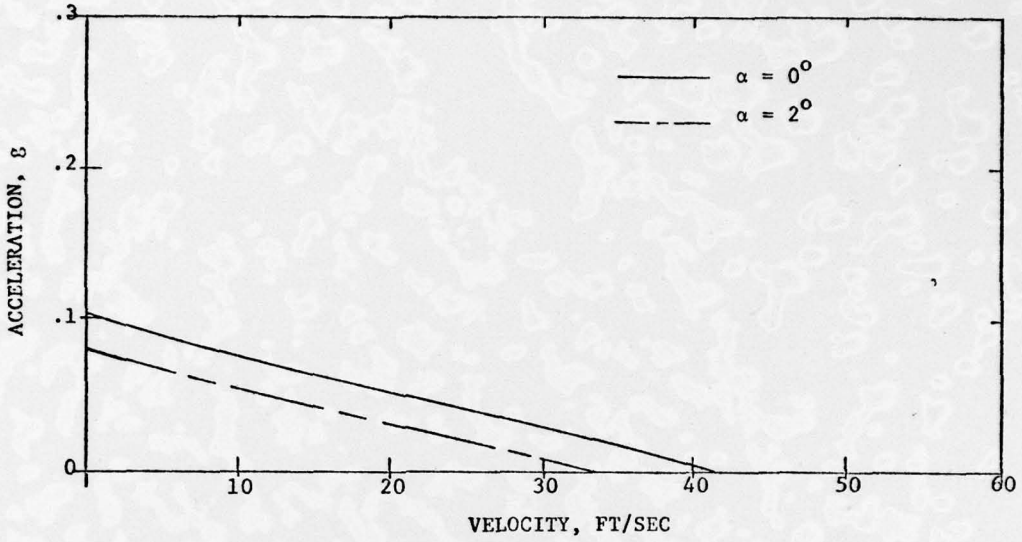


Figure 11 - Model Acceleration vs. Angle of Attack

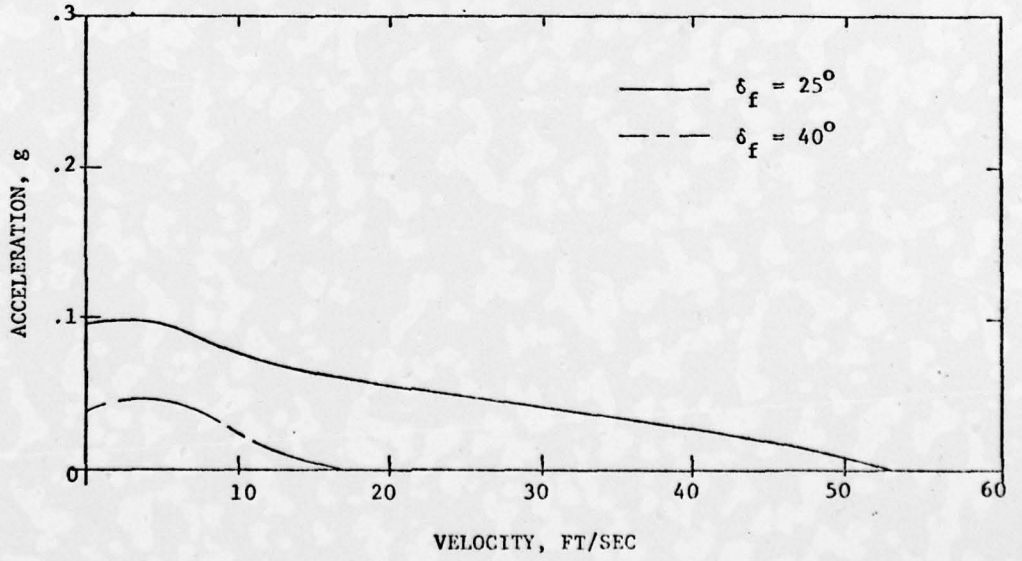


Figure 12 - Model Acceleration vs. Flap Angle

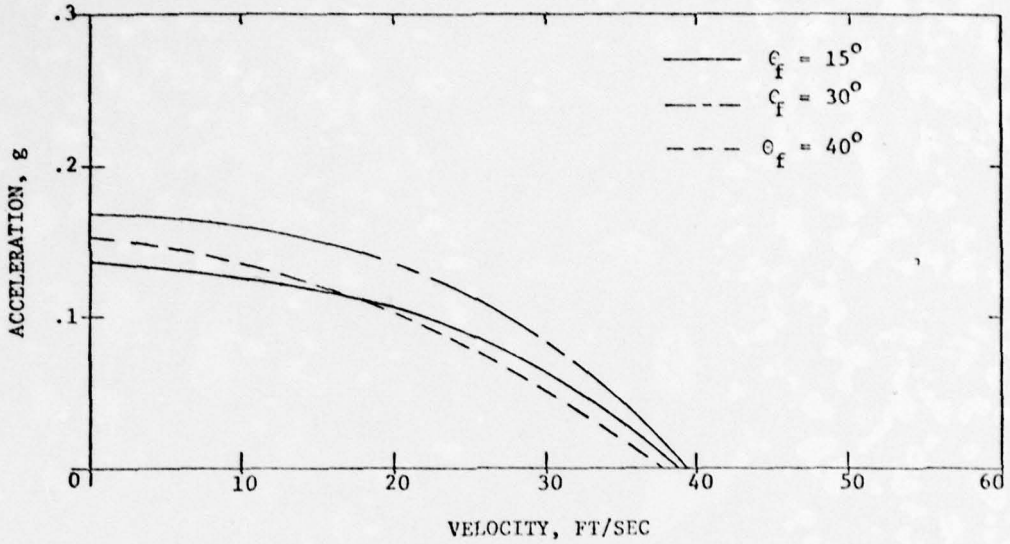


Figure 13 - Model Acceleration vs. Fan Angle

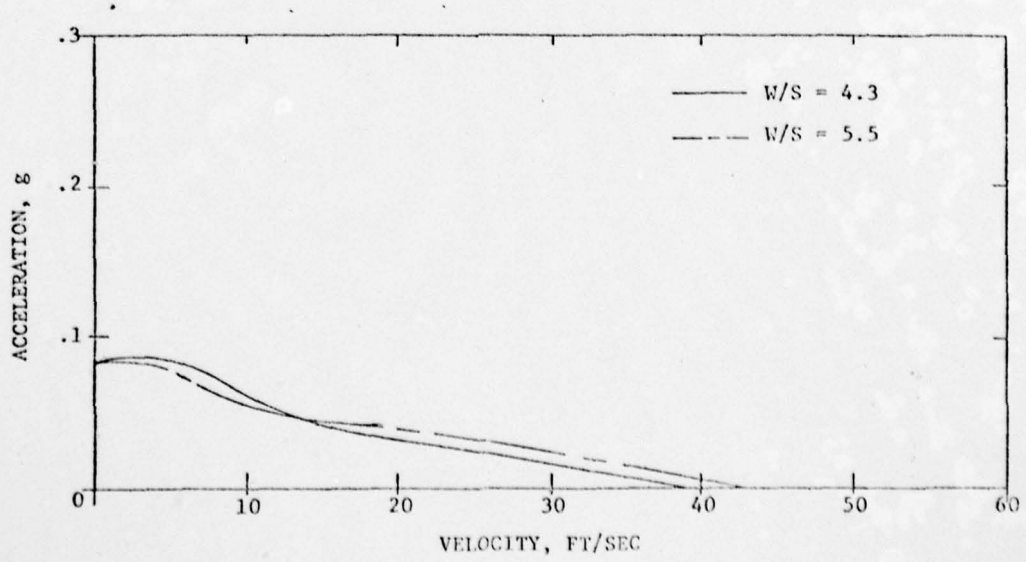


Figure 14 - Model Acceleration vs. Wing Loading

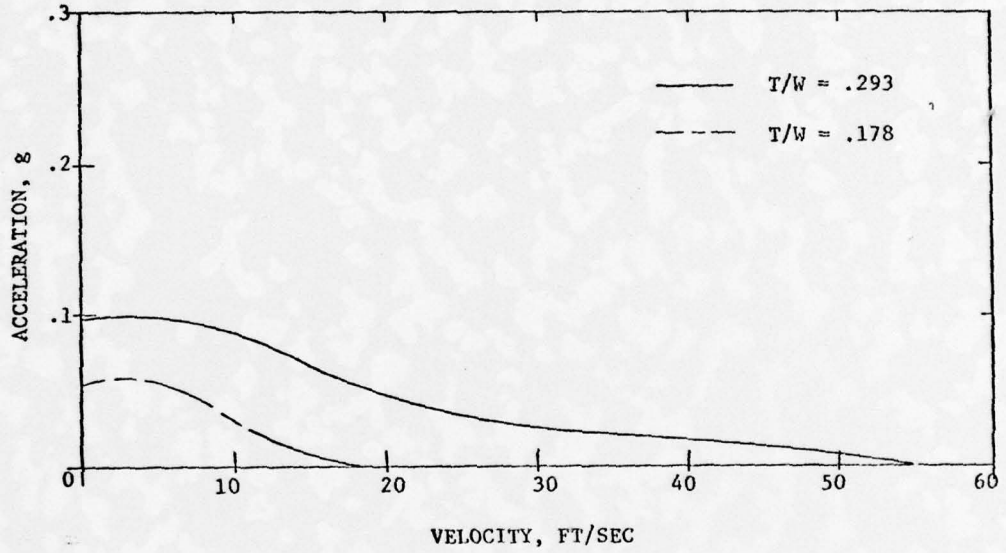
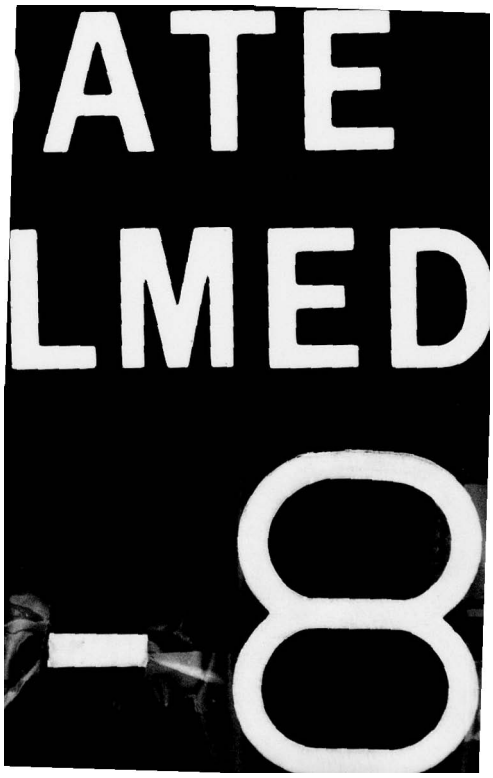


Figure 15 - Model Acceleration vs. Thrust Weight Ratio

TABLE 14 - RECOMMENDED AND HIGHEST ACTUAL PAR WIG SPECIFICATIONS

PARAMETER	RECOMMENDED	BEST ACTUAL (η_T = 31.3)
A	High ($\geq$ 2)	1/2
δ_f	0	20 (lowest)
Θ_f	Minimum	20 (lowest)
α	0	0
W/S	$\geq$ 5.5 lb/ft^2 (26.8 kg/m^2)	4.3 lb/ft^2 (21.0 kg/m^2)
T/W	$\geq$ .35	.357
$n_{f/b}$	$\geq$ 1 fan/ft (.3 fan/m)	1 (highest)


ATE
LMED
-8